Energy Storage Materials 67 (2024) 103248

Contents lists available at ScienceDirect

Energy Storage Materials

journal homepage: www.elsevier.com/locate/ensm

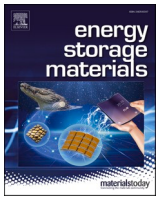

Strategies for pH regulation in aqueous zinc ion batteries

Mingqiang Liu [a,1], Peiqingfen Wang [b,1], Wei Zhang [d], Hongzhen He [a], Guanjie He [d], Shusheng Xu [b,*], Lu Yao [c,*], Thomas S. Miller [a,*]

[a] Electrochemical Innovation Lab, Department of Chemical Engineering, University College London, London, WC1E 7JE, UK
[b] School of Materials Science and Engineering, Shanghai University of Engineering Science, Shanghai 201620, PR China
[c] School of Materials Science and Engineering, Shanghai Institute of Technology, Shanghai 201418, PR China
[d] Department of Chemistry, University College London, London WC1E 7JE, UK

ARTICLE INFO

Keywords:
AZIBs
Zinc dendrites
HER
pH regulation
Electrolyte optimization

ABSTRACT

Aqueous zinc ions batteries (AZIBs), which use non-organic electrolytes, have garnered sustained interest as a future energy storage technology, primarily due to their low cost, environmental friendliness, and intrinsic safety. However, zinc ion batteries suffer from a series of serious challenges, including hydrogen evolution reaction (HER) at the anode, surface passivation, dendrite formation, as well as limited operating voltage and comparatively low energy density. These factors are all influenced by the concentration of H^+ in the electrolyte (i.e. the pH), and its fluctuations during the cycling process. To date, there remains a lack of systematic evaluation of the correlation between the pH value of electrolyte and the challenges faced by AZIBs, a focused review of how pH influences the electrochemical performance of AZIBs, or any focused discussion of strategies that can be used to improve cell efficiency. In this review we emphasize the strong correlation between electrolyte pH and AZIBs challenges and detail the research progress made in recent years relating to electrolyte additives, separator modification, interfacial protective layers, and battery system design, with a particular focus on the regulatory mechanisms associated with pH control. On this basis, we propose future research focuses and make suggestions for the onward development of AZIBs.

1. Introduction

While alkali ion batteries based on organic electrolytes, particularly lithium-ion batteries (LIBs) have undoubtedly revolutionized modern society, this family of energy storage systems are hindered by various challenges [1–6], including safety concerns related to organic electrolytes, insufficient or unsustainable material resources, escalating costs, and demanding assembly conditions. This has driven the recognition that other battery chemistries would be more appropriate for numerous applications and catalyzed a search for novel next-generation energy storage solutions [7]. Compared with LIBs with organic electrolytes, aqueous rechargeable batteries use water-based electrolytes characterized by higher ionic conductivity, enhanced safety, and reduced cost. Consequently, aqueous rechargeable batteries, utilizing a diverse range of charge carriers including Li^+, Na^+, K^+, Ca^{2+}, Mg^{2+}, Zn^{2+}, and Al^{3+}, have garnered significant attention and undergone extensive investigation [8–11]. While multivalent battery systems employing carriers such as Ca^{2+}, Mg^{2+}, and Al^{3+} exhibit higher theoretical capacities, the lower electrode redox potentials (−2.84, −2.36, −1.68 V vs. Standard Hydrogen Electrode, SHE) make them more prone to pronounced side reactions with water [12]. In contrast, metallic Zn possesses a high theoretical capacity (820 mAh g^{-1} or 5855 mAh cm^{-3}) in AZIBs. Additionally, Zn metal offers several advantages, including its abundancy, low cost, low toxicity, and comparatively high oxidation- and humidity-resistance when compared to alternative aqueous rechargeable battery anodes (e.g., Na and K). Furthermore, the use of Zn enables the direct assembly of AZIBs in ambient air, thereby reducing the manufacturing complexity and cost [13–15]. These favorable attributes make AZIBs a promising and practical alternative in the landscape of rechargeable battery technologies.

Despite the numerous advantages associated with AZIBs, their practical application is hindered by a series of challenges, which include hydrogen evolution (via the hydrogen evolution reaction, HER) at the anode, dendrites, corrosion, passivation and dissolution at the surface of

* Corresponding authors.
E-mail addresses: xushusheng@sues.edu.cn (S. Xu), luyao@sit.edu.cn (L. Yao), t.miller@ucl.ac.uk (T.S. Miller).
[1] P. Wang and M. Liu contributed equally to this work.

https://doi.org/10.1016/j.ensm.2024.103248
Received 27 December 2023; Received in revised form 29 January 2024; Accepted 4 February 2024
Available online 5 February 2024

zinc metal anode, and the generation of by-products at the cathode. Notably, a high concentration of H^+ ions in the environment (low pH) exacerbates side reactions such as the HER, corrosion, and anodic dissolution. Conversely, a high concentration of OH^- ions in the environment (high pH) expedites the formation of passivates and by-products at both the cathode and anode interfaces [16–18].

It is worth highlighting here that strongly alkaline electrolytes are rarely used for AZIBs, as in these conditions the mechanism shifts from a highly reversible deposition/stripping reaction of Zn^{2+} at the zinc anode to a reversible transformation reaction involving Zn, $Zn(OH)_4^{2-}$, and ZnO. While this can enable elevated output voltage, the challenges faced due to cell degradation are significantly more severe compared to AZIBs with mild electrolytes [19–21]. While in a strong acid electrolyte, Zn metal undergoes a rapid reaction with H^+, leading to anodic dissolution. Hence, AZIBs batteries conventionally control the pH range of the electrolyte within a mild range (weak acid or nearly neutral), so as to mitigate the occurrence of strong side-reactions. Unfortunately, HER is more significant in mild environments and depletes the H^+ at the metal/electrolyte interface, leading to a significant increase in the interfacial pH which gradually extends into the bulk phase. This means that a mild electrolyte pH will gradually deviate from the normal operating pH range in a long-term cycling, generating more severe problems leading to the failure of the battery. Furthermore, recent research [16–18] has also revealed that HER-induced interfacial pH fluctuations directly affect the Zn^{2+} deposition process, exacerbating zinc dendrite growth.

It is clear that all the challenges with AZIBs described above are intricately linked to the electrolyte pH. Therefore, the effect of electrolyte pH is significant on electrochemical performance of AZIBs (Fig. 1).

While there have been some reviews describing the differences between alkaline and mild AZIBs, two types of battery systems based on different electrolyte pH, in terms of operating environment, energy storage mechanism, etc., there has been less focus on the systematic correlation between the pH value of the electrolyte and the existing problems of AZIBs, as well as the deeper influence of pH on AZIBs electrochemical performance [19–21]. Thus, an imperative exists for further research efforts dedicated to elucidating the complex relationship between electrolyte pH and the multifaceted challenges encountered in AZIBs, ultimately contributing to a more profound understanding of the underlying electrochemical processes and advancing this promising energy storage technology.

In the sections below we first emphasize the correlation between the current challenges encountered by AZIBs and the pH value of the electrolyte. Subsequently, we turn to direct exploration of the causal relationship between alterations in electrolyte pH and apparent differences in the electrochemical performances of AZIBs and reveal the mechanisms underlying these changes. Factors including the energy storage mechanism at the electrodes, the redox potentials, the rate of the electrode reaction, as well as the ionic concentration and conductivity of the electrolyte, and the electrochemical stability window (ESW) are discussed. By scrutinizing these factors, we seek to reveal the complex dynamic response of AZIBs to changes in electrolyte pH, thereby contributing to a more comprehensive understanding of their electrochemical behavior. Finally, we highlight recent advancements in electrolyte pH regulation strategies to drive high stability AZIBs, proposing future directions for the development of more stable and higher capacity systems in the future.

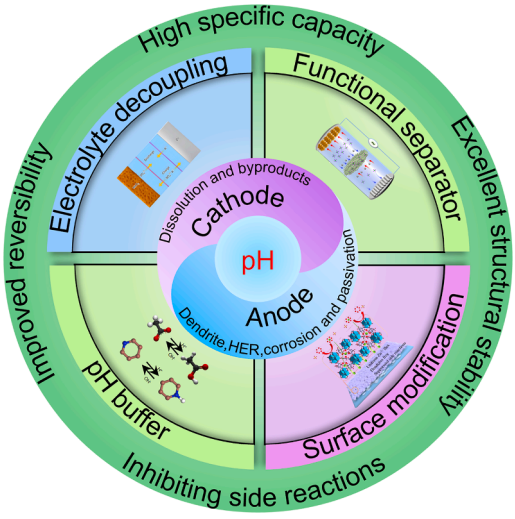

Fig. 1. Schematic diagram of the strategies for electrolyte pH regulation in AZIBs. Reproduced in part with permission from Ref. [22]. Copyright 2020 The Authors. Licensed exclusively to Springer Nature Limited. Reproduced in part with permission from Ref. [23]. Copyright 2023 Elsevier. Reproduced in part with permission from Ref. [24]. Copyright 2023 Elsevier.

2. Effect of pH on AZIBs

Currently AZIB research is heavily focused either on the development of new high-performance electrode materials, including novel cathodes (including manganese-based [25–28], vanadium-based [22–24,29,30], organics [31–38], prussian blue analogues [39–43], etc.) or protected zinc anodes [44–50], which can both deliver higher energy and power densities and improved electrochemical performance [51–53], or the development of strategies to stabilize AZIBs performance. Electrolyte modification, functionalized separators, and artificial interfacial layers have all been explored to improve Zn^{2+} deposition behavior, Zn^{2+} solvation structure, or Zn^{2+} insertion/extraction mechanisms. However, while these strategies have been shown to work, the problems associated with AZIBs are often closely linked to the microenvironment of the electrolyte, especially the local H^+ concentration at the electrode/electrolyte interface, and thus the correlation between the existing challenges of AZIBs and pH needs to be further elaborated to inform and guide developments [15,34].

2.1. Anode

The pH value of the electrolyte closely correlates with the reactions taking place at the zinc metal-anode interface, below these reactions are briefly introduced [54,55].

2.1.1. HER

HER refers to the process of electrochemical water decomposition to produce H_2. In AZIBs, HER needs to be avoided, but due to thermodynamic instabilities the HER inevitably occurs at the electrode/electrolyte interface of AZIBs, which leads to problems such as water depletion, gas production, and changes in electrolyte pH, which will significantly affect the electrochemical performance of the entire cell. The occurrence of HER is related to both the standard oxidation potential of the electrode and the pH value of the electrolyte. HER tends to occur more prominently at electrodes with lower redox potentials, particularly at the surface of the anode. As depicted in Fig. 2a, which illustrates the Pourbaix plot of zinc in aqueous solution, the standard reduction potential of Zn^{2+}/Zn is consistently below the equilibrium potential of H^+/H_2. Consequently, HER is inevitably initiated before the completion of the Zn^{2+} deposition process, making it challenging to entirely circumvent HER on the anode. Furthermore, it's noteworthy that the ESW of the aqueous electrolyte remains constant, irrelevant to the pH value. The HER and Zn deposition reactions in acidic electrolyte conditions are as follows:

Hydrogen evolution reaction (HER):

$$2H^+ + 2e^- \rightarrow H_2\uparrow (0\ V\ vs.\ SHE) \quad (1)$$

Zn deposition:

$$Zn^{2+} + 2e^- \rightarrow Zn(-0.762V\ vs.\ SHE,\ pH < 8) \quad (2)$$

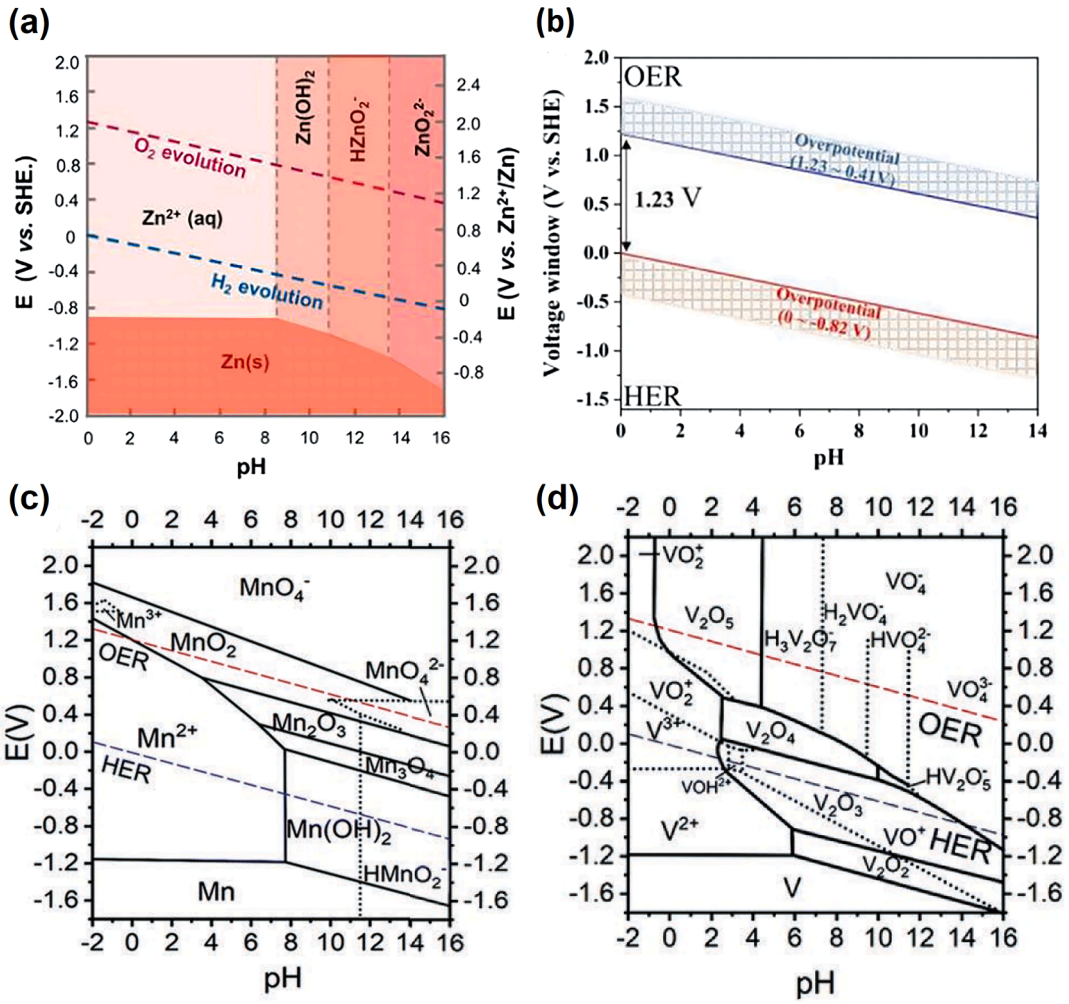

Fig. 2. Pourbaix diagram. Pourbaix diagram of (a) Zn metal in aqueous solution and (b) H_2O. Reprinted with permission from Ref. [56]. Copyright 2023 Willey-VCH. Pourbaix diagram for (c) manganese oxides and (d) vanadium oxides. Reprinted with permission from Ref. [57]. Copyright 2018 Willey-VCH.

It should be noted that there is a certain overpotential for HER (Fig. 2b), which makes the HER kinetics slower, and compared with other aqueous batteries, such as Mg (−2.37 vs. SHE), Ca (−2.87 V vs. SHE), and Al (−1.66 V vs. SHE), the higher standard redox potential of Zn (pH<8, −0.762 V vs. SHE) does enable the avoidance of the HER to some extent, but in the actual operation of AZIBs, the higher current density and the larger overpotential during charging still make HER possible [58].

The occurrence of HER is related to the pH value of the electrolyte. The overall reaction path of HER at different electrolyte pH values is different, with HER in acidic electrolyte proceeding according to Eq. (3), while in alkaline electrolyte according to Eq. (4) [59]. According to the Nernst equation (Eq. (5)), the HER potential in aqueous solution, $E_{HER} = -0.0592 \times pH$, thus favoring HER under lower pH conditions.

$$2H^+ + 2e^- \rightarrow H_2\uparrow E = 0V \ vs.\ SHE \tag{3}$$

$$2H_2O + 2e^- \rightarrow H_2 + 2OH^- E = -(0.059 \times pH)\ V \ vs.\ SHE \tag{4}$$

$$\varphi_{H^+/H_2} = \frac{RT}{2F}\ln\left(\frac{C(H^+)^2}{\frac{p(H_2)}{p^{\varnothing}}}\right) \tag{5}$$

Where R is the universal (ideal) gas constant (8.314 J/mol K); T is the temperature in Kelvin (K); F is the Faraday constant (96,485 C mol^{-1}); C (H^+) is the concentration of H^+ (mol L^{-1}), p(H_2) is the partial pressure of H_2 and $p^{\varnothing}$ is the standard pressure (1 atm)

It is generally believed that the rate of hydrogen generation is significantly inhibited when pH>3.2, therefore, AZIBs are usually operated in mild-weak or near-neutral electrolytes (pH=3~5) to avoid strong self-corrosion phenomena in strong acids as well as the formation of passivates such as zinc hydroxide sulphate ($Zn_4(OH)_6SO_4{\cdot}xH_2O$, ZHS) in alkali, in which HER potentials range from −0.177 V to −0.295 V. Since the Zn deposition potential is −0.762 V in these mild electrolytes, the presence of HER severely limits the ESW of the electrolyte, further limiting the operation voltage range. In addition, in a mild pH environment, Zn^{2+} is easily solvated by H_2O, forming the solvation sheath $[Zn(H_2O)_6]^{2+}$, which increases the energy barrier of the reduction reaction and decreases the required potential for the Zn/Zn^{2+} reduction [60].

The occurrence of HER can lead to various issues. Firstly, it may lead to electrolyte depletion problems. As the water content in the electrolyte decreases, the contact area between the electrolyte and the electrodes diminishes, thereby increasing the internal resistance of the battery. Consequently, this results in a reduction in the battery capacity and coulombic efficiency (CE) [61]. Moreover, the H_2 bubbles generated by HER tend to attach to the electrode surface, which not only hinders the nucleation process of Zn, leading to uneven zinc deposition and dendrite formation, but also results in the gradual formation of a porous layer on the surface of Zn under the interference of H_2, and this enlarged contact area between the Zn anode and the electrolyte will further exacerbate the generation of HER. In the case of a closed battery system, the

continuous generation of H_2 causes a gradual increase in the internal pressure of the battery, which may eventually surpass the critical pressure that the battery casing can withstand, leading to the disintegration of the battery. While it may not lead to spontaneous combustion and bursting of the battery like in the case of organic electrolyte LIBs, it still poses serious safety hazards [14].

The HER-induced pH change of the electrolyte is also worthy of attention, and this change can be divided into three stages. Initially, the weak occurrence of HER on the surface of zinc electrode causes a rapid increase in pH at the electrode/electrolyte interface, subsequently influencing the pH of the bulk electrolyte. In the second stage, when the pH at the interface is higher than 5.47, passivates are formed to inhibit the further pH escalation at some extent, resulting in a continuous fluctuation of electrolyte pH as a consequence of the balance between passivation and HER. In the third stage, at extended cycling times, exposure of newly deposited Zn to water triggers further HER, causing a continuous upward trend in pH. Importantly, the shift in pH values may trigger a cascade of problems throughout the extended cycling process. This poses a considerable challenge to the development of AZIBs with prolonged cycle life.

2.1.2. Dendrite growth

Zn dendrites refer to sharp structures formed by uneven deposition of metallic Zn from the reduction of Zn^{2+} on the bulk Zn anode surface, which can cause "dead zinc" and battery short circuits. The reasons for the uneven deposition of are complicated. In the initial stage of deposition, Zn^{2+} is reduced in a two-dimensional diffusion process, and Zn nuclei are formed at the most energetically favorable locations (tips, impurities, lattice defects, etc.) [61]. The nucleation of Zn is influenced by the electric field strength, ion concentration, and surface energy, collectively acting as a driving force to overcome the nucleation barrier. A localized area with a lower nucleation barrier and higher nucleation driving force is more prone to Zn nucleation, disrupting the uniform deposition of Zn across the entire area [58]. A typical example of this is the "tip effect", where higher current density near the curvature of the Zn surface generates a larger electric field driving force to complete the nucleation process, thus increasing the Zn nucleation mass in this region, further resulting in an overall uneven deposition of Zn. In addition, the tip effect also contributes to an uneven distribution of ion concentration, the larger electric field driving force near the tip accelerates the transformation of Zn^{2+} into Zn, while in the non-tip region, there is still a large aggregation of Zn^{2+}. This non-uniform distribution of ion concentration on the surface of the zinc will also lead to uneven Zn deposition [58,62]. During subsequent deposition, Zn^{2+} tends to be deposited on the existing surfaces with higher curvature to minimize the surface energy, thus accelerating dendrite growth [62].

Thus, the formation of dendrites is mainly attributed to the inhomogeneous deposition behavior of zinc ions, influenced by various factors such as nucleation overpotential, crystal orientation, electric field strength and ion concentration distributions, nucleation location, and Zn^{2+} flux [60]. However, the correlation and influence of electrolyte pH on zinc deposition behavior is often neglected. Zinc has high solubility, electrochemical activity and thermodynamic instability in alkaline electrolytes, Zn therefore exhibits pronounced dendritic growth under alkaline pH conditions. Compared with alkaline conditions, the formation of dendrites in AZIBs in mild pH electrolyte is effectively suppressed due to the reversible redox reaction of Zn^{2+}/Zn, but the repeated deposition/stripping makes it challenging to entirely avoid zinc dendrites[59]. First, H_2 generated at lower pH and ZHS passivates formed at higher pH affect the process of Zn^{2+} deposition. Second, in a lower pH environment, the zinc electrode is more likely to undergo self-corrosion, which is due to the fact that trace impurities are dispersed in the electrolyte, affecting the uniform distribution of the electric field [63]. Moreover, the pH of the electrolyte also affects the morphology of dendrites, in a lower pH environment, Zn^{2+} tends to undergo three-dimensional nucleation. As the pH increases, the nucleation mechanism changes to two-dimensional nucleation, which significantly affects the morphology, number and size of the final Zn dendrites. This, in turn, affects the morphology of the Zn deposition in the surrounding flat area. Considering that the electrolyte pH value continues to change under the influence of the HER, the Zn deposition environment becomes more complex in different areas, exacerbating the formation of Zn dendrites [63]. Furthermore, the change in pH due to HER can directly affect the uniform deposition process of Zn by changing the distribution of ion concentration in the electrolyte and Zn^{2+} flux to trigger dendrites, which has not received sufficient attention.

Dendrites cause several problems in AZIBs. Firstly, Zn dendrites, being brittle and prone to fracture upon reaching a certain level of growth, lead to the formation of disconnected and isolated metallic Zn, which leads to the irreversible loss of Zn and reduces the CE. The sharp edges of dendrites can pierce the separator and increase the risk of short-circuit. While these short circuits aren't as hazardous as those in lithium-ion batteries with organic electrolytes, this problem also greatly shortens the life of AZIBs. Moreover, the formation of dendrites increases the contact area between the zinc anode and electrolyte, thus providing more reaction sites for issues such as HER, corrosion and passivation, which in turn exacerbate the formation of dendrites by generating H_2 and altering the pH value of the electrolyte.

2.1.3. Corrosion and passivation

The corrosion of the zinc metal surface usually occurs simultaneously with HER through the formation of numerous microcells at the interface of the two phases, causing the metal Zn to lose electrons to Zn^{2+} dissolved in the electrolyte (Eq. (6))[58]. The occurrence of corrosion is closely linked to the pH of the electrolyte, with more severe corrosion observed in strong acid and alkaline environments compared to mild environments. It should be noted that although Zn also undergoes strong corrosion under alkaline environment, the dense by-product ZnO formed in the alkaline environment will work as a protective layer cover the surface of the anode, which to a certain extent isolates the Zn metal from the electrolyte, inhibiting further Zn corrosion. But there is no condition for the formation of dense protective film under strong acid environment. Even in weak acid environments, such as $ZnSO_4$ for example, the corrosion by-product ZHS forms within a certain pH range, but the loose structure produced by the discontinuous ZHS formation process due to the change of pH does not effectively prevent the contact between the surface of the zinc metal and the electrolyte [64–66].

Zinc corrosion:

$$Zn + 2H^+ \rightarrow H_2\uparrow + Zn^{2+} \quad (6)$$

Passivation is mainly caused by electrochemically inert materials (e.g., $Zn_4(OH)_6$ $SO_4{\cdot}xH_2O$, ZnO, $Zn(OH)_2$) generated during battery charging and discharging processes, which are usually deposited on the surface of the Zn electrode, reducing the active surface area of the Zn electrode and inhibiting the charge transfer kinetics at the electrode surface, leading to an irreversible loss of capacity and a reduction in the CE as well as the cycle life.

There is a significant relationship between electrolyte pH and passivation, first of all, the passivates formed under different electrolyte pH levels vary. Experimental evidence shows that when using $ZnSO_4$ electrolyte, the main passivate under acidic condition is ZHS, while the main passivate is $Zn(OH)_2$ in a weak alkaline environment with pH>8.5 (Fig. 2a). In a strong alkaline electrolyte the main passivate is ZnO. As AZIBs usually use a mild electrolyte (pH=3~5), under normal conditions passivation does not occur. However, when HER causes the pH to fluctuate to >5.47, Zn^{2+} combines with SO_4^{2-}, H_2O, and OH^- in the electrolyte to form ZHS [67]. The mechanisms of passivation byproduct formation at different pHs are as follows:

Formation of alkaline environmental passivates:

$$Zn - 2e^- + 4OH^- \rightarrow Zn(OH)_4^{2-} \quad (7)$$

$$Zn(OH)_4^{2-} \rightarrow ZnO + H_2O + 2OH^- \quad (8)$$

Formation of acidic environmental passivates:

$$Zn - 2e^- \rightarrow Zn^{2+} \quad (9)$$

$$4Zn^{2+} + 6OH^- + SO_4^{2-} + xH_2O \rightarrow Zn_4SO_4(OH)_6 \cdot H_2O \quad (10)$$

For AZIBs, the nature of the relationship between passivation and pH is due to OH^-critical solubility [12]. When the concentration of OH^- in the electrolyte reaches the critical solubility, OH^- cannot be dissolved in water and thus precipitates as ZHS. The critical solubility of OH^- is calculated as follows:

$$C(OH^-) = 6\sqrt{\frac{K_{sp}(Zn_4SO_4(OH)_6 \cdot nH_2O)}{C([Zn(H_2O)_6]^{2+})^4 \cdot C(SO_4^{2-})}} \quad (11)$$

where K_{sp} is the solubility product constant, calculated as follows:

$$K_{sp}(Zn_4SO_4(OH)_6 \cdot nH_2O) = C([Zn(H_2O)_6]^{2+})^4 \cdot C(OH^-)^6 \cdot C(SO_4^{2-}) \quad (12)$$

The corrosion and passivation processes in AZIBs during charging and discharging are closely related to the CE and cycling stability. Firstly, the formation of ZHS comes at the expense of consuming Zn^{2+}, leading to irreversible capacity loss of Zn [66]. Secondly passivation, which covers the surface of the Zn surface, increases the internal resistance of AZIBs and reduces the energy efficiency. Finally, ZHS hinders the homogeneous deposition of carrier Zn^{2+} and the formation of reversible products. This not only reduces the reversibility of charging and discharging but also impacts the Zn flux, accelerating the growth of dendrites [59]. Although the passivate for AZIBs in mild systems is mainly ZHS, considering the rise in pH due to HER and the limited ability of ZHS to inhibit pH changes, passivates like ZnO and $Zn(OH)_2$ in alkaline systems should also be taken into account during the engineering of AZIBs with a long cyclic life, particularly when implementing effective pH regulation strategies.

2.2. Cathode

As with the anode, pH has a strong influence on cathode reactions. Below key concepts are introduced.

2.2.1. Cathode dissolution

The pH of the electrolyte plays a crucial role in determining the electrochemical stability of the cathode material in AZIBs. An unsuitable pH environment can lead to structural degradation and disintegration of the cathode material, impacting the overall performance and cycling life of the battery.

Taking the MnO_2 cathode as an example, the Pourbaix diagram of Mn oxides, as shown in Fig. 2c, reveals that in a mild electrolyte system (pH = 3~5) below 0.8 V, Mn oxides are dissolved in the electrolyte in the form of Mn^{2+}. Notably, the lower the electrolyte pH, the higher the redox potential of Mn^{2+}/MnO_2, leading to easier dissolution. Consequently, in AZIBs utilizing acidic electrolytes, manganese inevitably dissolves from the active material into the electrolyte, significantly impacting the sustainability of manganese-based electrode materials. The loss of manganese in the active material leads to the structural degradation of the electrode and capacity decay [68].

Vanadium-based oxides also suffer from the problem of active material dissolution. Compared with manganese-based oxides, the dissolution behavior of vanadium-based oxides is more complex due to the multivalent nature of V (V^{2+}, V^{3+}, and V^{5+}), but is still correlated with the pH value. As shown in the Pourbaix diagram of vanadium-based oxides (Fig. 2d) [69] vanadium mainly dissolves in the electrolyte as VO^{2+} when pH<3 and the electrode potential of vanadium-based oxides is lower than 0.45 V (vs. SHE), vanadium predominantly dissolves in the electrolyte as VO^{2+}. In the pH range of 3 to 6, vanadium predominantly dissolves in the electrolyte as VOH^{2+} and a lower potential is required to complete the conversion (−0.05 V vs. SHE for pH = 3, −0.60 V vs. SHE for pH = 6). When the electrode potential is above 0.4 V, $H_3V_2O_7^-$ is the main dissolved species [69]. The form of the dissolved substance will have an effect on the energy storage mechanism of the anode, and it may also diffuse to the Zn anode to be reduced to V^{3+} or V^{4+} and deposited on the Zn, which reduces the available electrochemical reaction sites and decreases the electrode utilization [70].

2.2.2. Byproducts

Similar to corrosion derived ZHS byproduct deposition on the surface of metal anode, layered double hydroxides (LDH) are commonly formed on the surface of the cathode material during the discharge process. The precipitation of these LDHs in the $ZnSO_4$ electrolyte is closely related to the pH value. During the discharge process, H^+ can also insert into the cathode material, resulting in a localized pH increase at the cathode/electrolyte interface, which ultimately produces LDH (pH=5.47) as OH^- accumulates. In addition, during the charging process, H^+ tends to be reversibly extracted from the cathode material, subsequently lowering the electrolyte pH and stabilizing the pH at the cathode/electrolyte interface. Nevertheless, in the case of AZIBs undergoing prolonged cycling, the LDH layer will gradually accumulate or detach at the electrode surface, resulting in volume expansion and capacity decay of the cathode, and permanent depletion of the aqueous electrolyte.

2.2.3. Energy storage mechanism

The electrolyte pH value affects the energy storage mechanism of the cathode, thereby also influencing the electrochemical performance of AZIBs [71]. For Mn-based anodes, Lee et al. demonstrated that the change of electrolyte pH plays a key role in the reversible deposition/dissolution reaction on α-MnO_2 electrodes by monitoring the change of electrolyte pH (Fig. 3a) [67]. During the discharge process, MnO_2 is first electrochemically reduced to Mn^{3+} ($Mn^{4+}+e^- \rightarrow Mn^{3+}$), and the electronic configuration of the high spin of Mn^{3+} is usually unstable, so it will undergo a disproportionation reaction to Mn^{2+}, and the initial reaction at the cathode can be expressed by Eq:

$$MnO_2 + 2H_2O + 2e^- \rightarrow Mn^{2+} + 4OH^- \quad (13)$$

The continuous dissolution of manganese during the discharge process results in the continuous generation of OH^- ions, leading to an increase in the pH value of the electrolyte. Similarly, during the charging process, the continuous oxidation of manganese causes a continuous decrease in the pH value of the electrolyte.

In situ electrolyte pH monitoring (Fig. 3b) was used to obtain the change of electrolyte pH during the cycling process (Fig. 3c). The in situ X-ray diffraction (XRD) and its corresponding charge/discharge curves confirmed the reversible deposition/dissolution of ZHS on the cathode surface during battery charging and discharging, which was consistent with the change in pH. This conversion reaction related to the pH of the electrolyte can be expressed by Eq:

$$3MnO_2 + 8Zn^{2+} + 2SO_4^{2-} + 16H_2O + 6e^- \rightarrow 3Mn^{2+} + 2Zn_4(OH)_6(SO_4) \cdot 5H_2O\downarrow \quad (14)$$

This dissolution/deposition energy storage mechanism associated with the change of electrolyte pH has been further investigated, for example by Wu et al., who revealed for the first time by operando X-ray fluorescence mapping measurements that in the weakly acidic pH-based environment the main charge storage mechanism of α-MnO_2 is the dissolution deposition reaction of Mn^{2+}, which is quite different from the commonly considered insertion energy storage mechanism of H^+ or Zn^{2+} in the cathode [72]. More importantly, in situ based pH monitoring showed that the charge storage mechanism of ZHS deposition/dissolution during battery discharge/charging is dependent on the electrolyte-induced local pH changes during cycling. And the capacity retention in charge/discharge is highly correlated with whether the

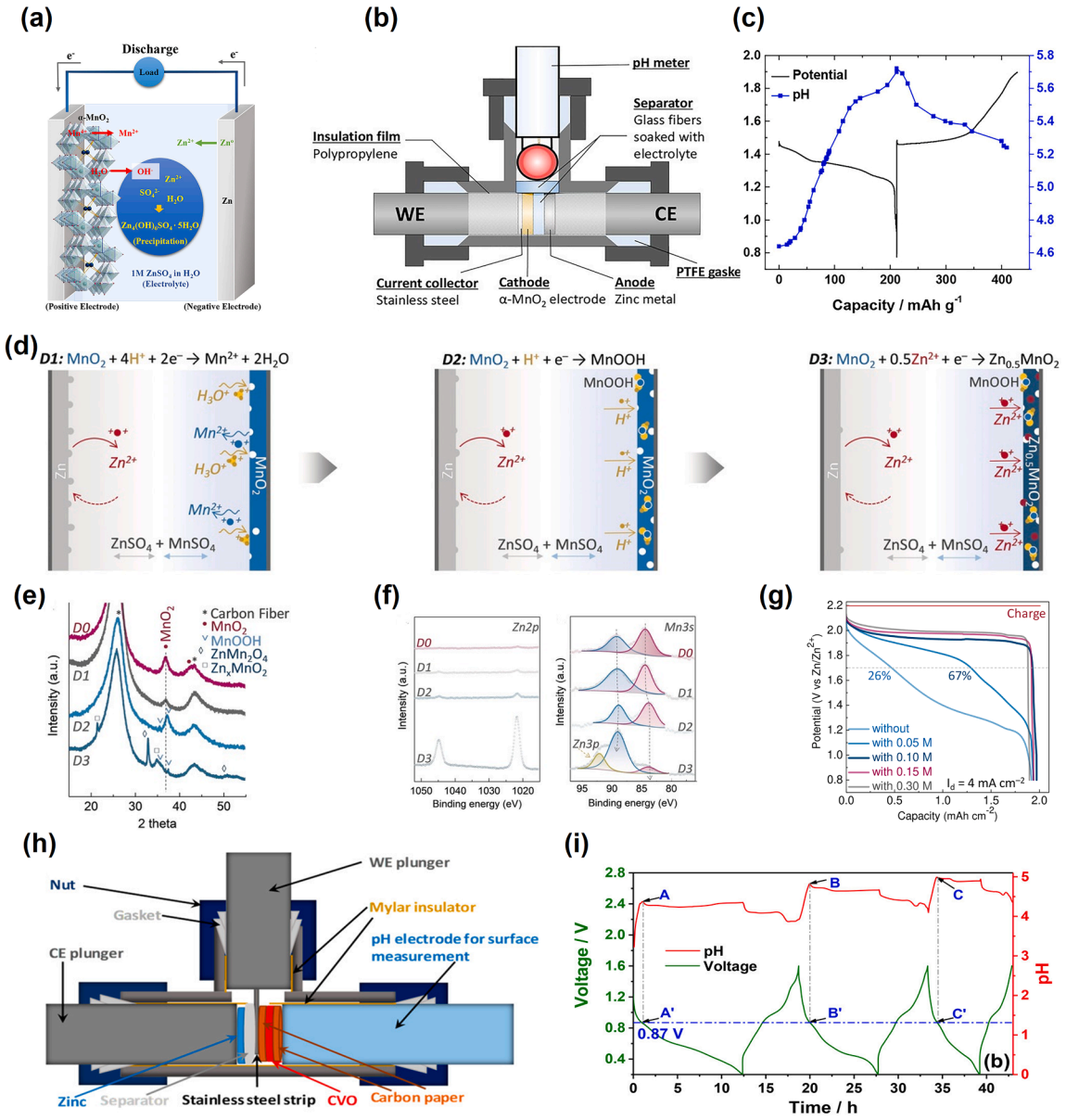

Fig. 3. Effect of electrolyte pH on cathode. (a) Energy storage mechanism diagram in α-MnO_2/Zn cells relies on the reversible dissolution/deposition process of ZHS, triggered by pH changes. (b) Experimental equipment for in situ pH monitoring during the electrochemical reaction in the α-MnO_2/Zn cell. (c) Evolution of electrolyte pH during the first discharge–charge process. Reprinted with permission from Ref. [72]. Copyright 2016 Willey-VCH. (d) Charge storage mechanism of the electrolytic Zn-MnO_2 battery in different pH. Ex situ (e) XRD and (f) XPS patterns of the MnO_2 cathode at various discharge states. (g) Galvanostatic discharge curves of electrolytic battery in electrolytes with x M H_2SO_4 (different pH). Reprinted with permission from Ref. [73]. Copyright 2019 Willey-VCH. (h) Experimental equipment for operando pH measurements. (i) Evolution of electrolyte pH and cell during the initial three discharge- charge process. Reprinted with permission from Ref. [74]. Copyright 2020 American Chemical Society.

electrolyte pH changes can induce the dissolution/deposition reactions of ZHS and Mn.

More importantly, altering the electrolyte pH by the use of acid electrolytes, such as acetate electrolytes or electrolyte additives can trigger the redox reaction of Mn^{4+}/Mn^{2+} (Fig. 3d), which can be verified by in situ XRD (Fig. 3e) and X-ray Photoelectron Spectroscopy (XPS) (Fig. 3f), and thus provide additional electrochemical specific capacity for AZIBs (Fig. 3g). It is essential to note that a lower electrolyte pH is not intrinsically better, because a low pH means a strong HER reaction on the anode, causing a reduction in CE and cycle life. A recent study [56] of a Zn/MnO_2 flow battery based on the Zn^{2+}/Zn deposition/stripping reaction and Mn^{2+}/MnO_2 dissolution/deposition reaction showed that both Zn^{2+} and H^+ participate in the energy storage process of MnO_2 at low discharge rate, engaging in a competitive relationship, whereas at high discharge current, H^+ even dominates in the reaction with MnO_2. This suggests that the electrolyte pH affects the reaction process between H^+, Zn^{2+} and MnO_2 through the H^+ concentration.

Vanadium-based materials stand out as one of the most promising cathodes for AZIBs, and their energy storage mechanism is also affected by electrolyte pH. Currently, the insertion/extraction mechanisms of Zn^{2+} and H^+ in vanadium-based oxides, especially for δ-V_2O_5 remain a subject of controversy, where conventional structural and elemental characterization methods face limitations in adequately distinguish the intercalation process of H^+ and Zn^{2+} in a 1 M $Zn(CF_3SO_3)_2$ aqueous electrolyte. Liu [57] developed an operando pH detection method for a Zn||δ-V_2O_5 cell (Fig. 3h), and demonstrated that H^+ and Zn^{2+} would be simultaneously inserted into δ-V_2O_5 and revealed an H^+/Zn^{2+} exchange

insertion/extraction mechanism. The experimental results showed that the pH evolution during cycling was significantly correlated with the battery voltage (Fig. 3i). The insertion of H^+ in the cathode during discharging is the main reason for the increase of the electrolyte pH value. Conversely, during charging, H^+ and Zn^{2+} will be extracted from the cathode, at which time the extracted H^+ becomes the primary factor contributing to the decrease in electrolyte pH. To deepen the understanding of the H^+/Zn^{2+} exchange insertion/extraction mechanism, it was found by density functional theory (DFT) calculations that at the same temperature and pressure, a higher H^+ concentration in the electrolyte causes more H^+ to be inserted into the cathode and exchanged with the Zn^{2+}, causing a decrease in the pH of the electrolyte. Whereas, in an electrolyte with high pH, the H^+ in the interlayer of cathode will in turn be exchanged with Zn^{2+} in electrolyte, making the electrolyte pH decrease. Due to the distinct kinetic rates of electrochemical reactions for the two different charge carriers, Zn^{2+} and H^+, the varying H^+/Zn^{2+} ratios resulting from different pH values notably impact the electrochemical performance of AZIBs, particularly in terms of rate performance. Consequently, on one hand, this charge storage mechanism involving H^+ influences the pH of the electrode/electrolyte interface. On the other hand, changes in the pH of the electrolyte will in turn affect the energy storage mechanism of the electrode. pH may also affect the electrochemical performance of organic cathodes by influencing their charge storage mechanism. However, excessive H^+ tends to cause structural changes to the organic materials during the charging and discharging process, leading to a sudden drop in battery performance or even failure. Na et al. demonstrate that H^+ plays a key influence on the cycling stability of organic cathode 1,4,5,8-naphthalene diimide (NDI) [75]. Electron transfer at NDI electrodes occurs through surface binding of carriers and subsequent solid-state diffusion. In a weak acid electrolyte, the insertion of H^+ into the NDI electrode becomes more pronounced with increasing current density, which accelerates the solvation process of NDI and leads to the dissolution of NDI molecules. The poorer cycling stability of the NDI anode is attributed to excess H^+ insertion at a higher discharge depth. Although experiments have shown that sacrificing the depth of discharge can provide higher cycle life, this comes at the expense of charge/discharge specific capacity. Modulation of the local cathode/electrolyte interface pH value and the amount of H^+ insertion is promising to ensure the charge/discharge specific capacity and rate performance while concurrently improving cycling stability.

Additionally, the electrolyte pH value also influences the dissolution/deposition potential of the cathode, which in turn affects the operating voltage of the battery. The relationship between electrolyte pH and electrode redox potential can be obtained from the Nernst equation. Taking MnO_2 as an example, according to the Pourbaix diagram (Fig. 2c), the smaller the pH, the higher the standard redox potential of the anode. Therefore, Zn/MnO_2 cells under a strong acidic environment are favorable for obtaining higher voltage and energy density [69,70].

2.3. Electrolyte

The electrolyte pH plays a crucial role in influencing the ESW of the electrolyte, subsequently affecting the operating voltage and energy density of AZIBs. The ESW of aqueous electrolytes faces limitations imposed by two kinetic processes linked to water decomposition: HER and the Oxygen Evolution Reaction (OER). A low pH reduces the HER potential, promoting HER occurrence at the anode/electrolyte interface. Conversely, a high pH elevates the OER potential, favoring OER occurrence at the cathode/electrolyte interface. The electrolyte pH affects the electrode redox potential, and the operating voltage and energy density of AZIBs are limited by the combined effect of redox potential of the electrode and the ESW of the electrolyte [76]. AZIBs possess higher cathode redox potentials and lower OER potentials in an acidic environment, as well as higher anode redox potentials and lower HER potentials under alkaline conditions. Therefore, to improve the stability of AZIBs, different electrolyte pH values require distinct suitable operating voltages [74,76–80].

3. pH regulation strategies

Given the significant impact of electrolyte pH on the electrochemical performance of AZIBs, various strategies have been implemented to regulate pH to improve their electrochemical performance. These strategies include electrolyte optimization, separator modification, and artificial interfacial protective layers (AIPLs).

3.1. Electrolyte optimization

Electrolyte optimization, as a part of electrolyte engineering, has been widely studied owing to its inherent simplicity, cost-effectiveness, and wide availability [73,81,82]. Electrolyte additives can improve the electrochemical performance of AZIBs by regulating or controlling the pH value of the electrolyte, and they can be broadly categorized into three types: acid/base pH regulators, buffer solutions, and nitrogen-containing heterocyclic organics. Acid/base pH modifiers, usually comprising strong acids or bases, drive a significant alteration in the initial pH of the electrolyte. In contrast, buffer solutions use buffer pairs formed by, for example, a weak acid and its conjugate base, a weak base and its conjugate acid, or acid salts and their secondary salts, dynamically control the concentration of H^+ and OH^- in the electrolyte, thus regulating and stabilizing the pH of an electrolyte at a certain value. Buffers can therefore stabilize the electrode environment and inhibit side reactions. Although nitrogen-containing heterocyclic organic compounds are similar to buffer solutions in regulating and stabilizing the pH value of the electrolyte, they mainly rely on the functional groups on the molecule chains to regulate the pH value, so the regulation mechanism is different.

In addition, electrolyte decoupling emerges as a pivotal method, facilitating the separation of different pH electrolytes and situating cathode and anode in acidic and alkaline environments, respectively. This approach ensures the provision of optimal pH environments for both the cathode and anode, thereby enhancing both cathode and anode redox potentials, expanding the ESW of the electrolyte, and improving the energy density of the battery.

3.1.1. Acid-alkali pH regulator

The initial pH value of the electrolyte can be significantly changed by adding a certain amount of acidic or alkaline pH modifiers to the conventional electrolyte in advance, which can improve the operation environment of electrodes and electrolyte. Chao et al. added a small amount of acid-base pH modifier, H_2SO_4, to a zinc/manganese sulfate-based electrolyte in order to significantly reduce the pH value of the electrolyte (pH < 1.5), and the assembled Zn-MnO_2 cells exhibited a discharge specific capacity of up to 507 mAh g^{-1} and a high operating voltage of 1.95 V, much higher than in conventional electrolytes [83]. The significant enhancement of the discharge capacity was attributed to the fact that the higher H^+ concentration at low pH can trigger the additional Mn^{4+}/Mn^{2+} two-electron redox reaction (Fig. 3d). The significant increase in operating voltage was attributed to the low electrolyte pH increasing the dissolution deposition potential of anodic MnO_2. It is worth noting that a lower electrolyte pH does not necessarily imply superior performance, and experiments have shown that when the electrolyte pH is in the range of 1.1–4.6, the capacity contribution to the high-voltage region (2.0–1.7 V) where two-electron redox occurs, shows a nonlinear increase in capacity contribution to the CE with the decrease of electrolyte pH (Fig. 3g). However, when the electrolyte pH was less than 1, this changing relationship showed a significant turnaround and the capacity contribution rate and CE began to decrease as the pH continued to decrease (Fig. 3g). This turnaround is mainly attributed to the strong HER caused by the low pH, which reduces the HER potential and consequently narrows the ESW of the electrolyte, causing Zn-MnO_2

to suffer more negative effects from the HER in the high-voltage region. Therefore, a 0.1 M concentration of H_2SO_4 electrolyte additive was chosen as a trade-off between stability and voltage performance to obtain a stable potential window of up to 2.41 V with a high discharge plateau and CE.

In addition, lowering the electrolyte pH by acid-base pH modifiers plays a role in delaying the formation of ZHS. Zhang et al. reduced the electrolyte pH by adding H_2SO_4 to $ZnSO_4$ (pH = 4.29 → 2.8) and found that the $ZnSO_4$ electrolyte pH increased significantly from 4.29 to 5.6 within the first 6 h and fluctuated thereafter, and that the initial pH The significant increase was attributed to HER, while the subsequent fluctuation in pH was due to the competition between HER and ZHS formation [84]. However, for the H_2SO_4-added electrolyte, the increase in pH from 2.8 to 5.63 took 18 h. Since the formation of ZHS generally requires a sufficient OH^- concentration (pH ≈ 5.47), a lower electrolyte pH can delay the formation of ZHS. Nevertheless, it is worth noting that this strategy did not enhance the cycle life of the AZIBs, and the batteries with both electrolyte compositions have been shown to be prone to short-circuit within a relatively short period of time. Low pH delays the formation of ZHS, but stimulates the occurrence of HER, more

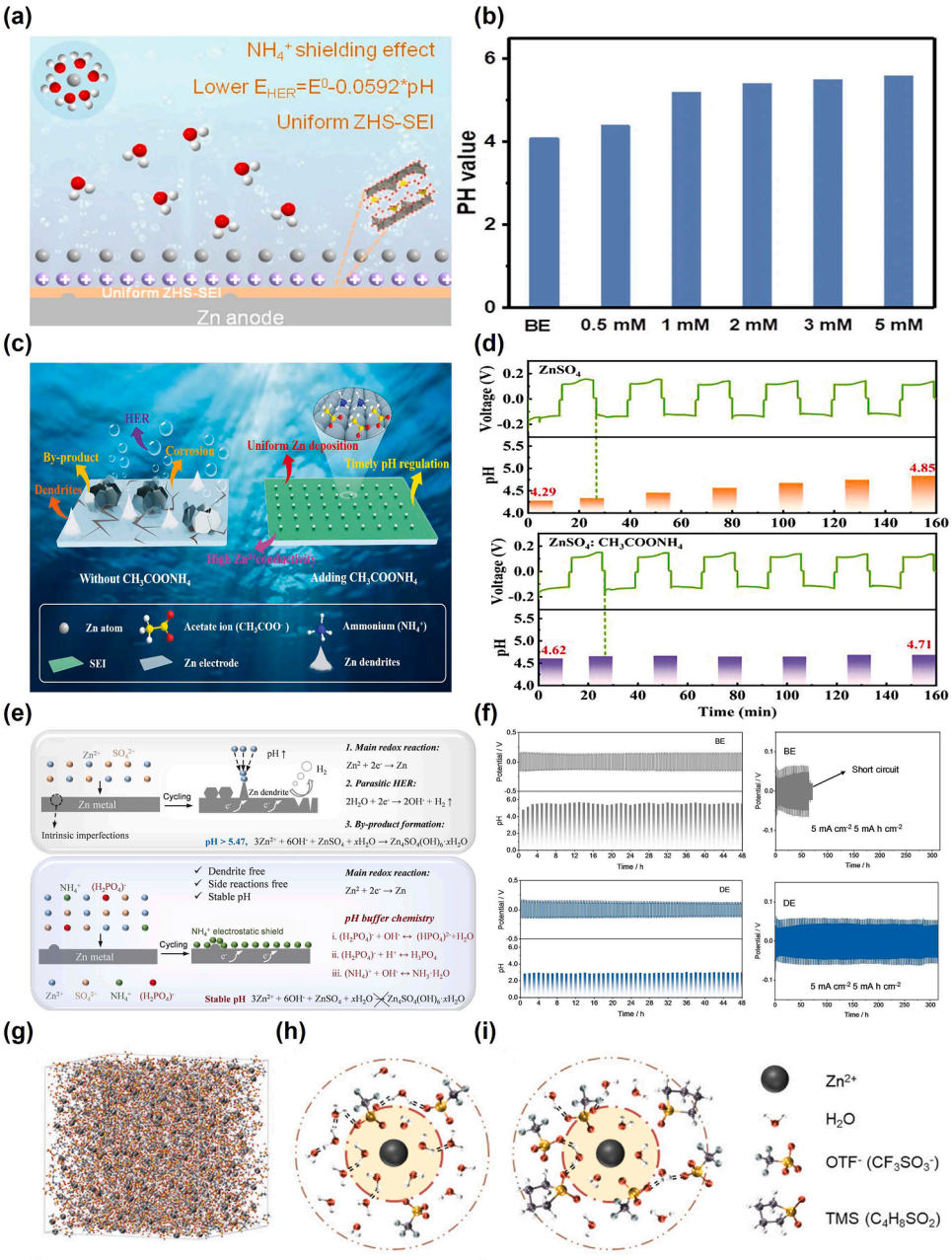

Fig. 4. Regulating electrolyte pH with acid-alkali pH regulator or buffer solutions. (a) Schematic illustrations of Zn deposition process under pH regulation by ammonium hydroxide. (b) pH values evolution in different concentration ammonium hydroxide. Reprinted with permission from Ref. [86]. Copyright 2023 The Authors. (c) Schematic illustration of the zinc deposition process on the anode without or with the NH_4OAc additive. (d) pH values evolution in 2 M $ZnSO_4$ electrolyte without or with NH_4OAc of symmetric batteries cycling at 5 mA cm^{-2}, respectively. Reprinted with permission from Ref. [87]. Copyright 2022 The Authors. Published by Willey-VCH. (e) Mechanism diagram of dihydrogen phosphate (NHP) additives inhibiting Zn anode existing problems. (f) pH values evolution in 1 M $ZnSO_4$ electrolyte without (BE) or with 25 mM NHP (DE) of symmetric batteries cycling at 10 mA cm^{-2}, respectively. Reprinted with permission from Ref. [88]. Copyright 2022 The Authors. Published by Willey-VCH. (g) 3D snapshot of 3 M $Zn(OTF)_2$-H_2O/ tetramethylene sulfone (TMS) (5:5) electrolyte obtained from molecular dynamics (MD) simulations. Schematic illustrations of typical coordination structures for 3M $Zn(OTF)_2$-H_2O with (h) and without (i) TMS. Reprinted with permission from Ref. [89]. Copyright 2022 Willey-VCH.

importantly, the stronger tendency of HER in the low-pH environment also in turn increases pH value at the same time, which leads to the pH value for the formation of ZHS very quickly. Chen et al. added a trace amount of a trifunctional electrolyte additive, ammonium hydroxide, to the $ZnSO_4$ electrolyte thereby constructing a ZHS-based solid electrolyte interphase (SEI) on the surface of zinc anode in situ (Fig. 4a) [85]. First, ammonium hydroxide increases the pH value of the electrolyte (pH = 4.1 → 5.2, 1 mM) (Fig. 4b). According to the Nernst equation (Eq. (5)), the increase of pH can reduce the potential of HER and thus inhibit the occurrence of HER to a certain extent. Besides, NH_4^+ in ammonium hydroxide can be preferentially adsorbed on the surface of the Zn metal, shielding the "tip effect" and homogenizing the electric field distribution, thus fostering a more uniform Zn deposition. Due to this comprehensive protection, dendrite-free anode and highly reversible Zn stripping/plating behavior were achieved. It is particularly important to note that the ZHS here serves to inhibit corrosion and improves the transport kinetics of Zn^{2+}. This is significantly different from what we generally think of as the role of ZHS. This is mainly due to the fact that the formation rate of ZHS is related to the electrolyte pH. In a weak acidic environment (e.g., $ZnSO_4$), the increase of pH resulting from HER initiates the gradual formation of a ZHS-based SEI on the surface of Zn metal. This SEI structure is loose, and make it difficult to fully isolate the metal anode from the electrolyte, and consequently fails to effectively inhibit corrosion.

However, if the initial pH of the electrolyte is elevated, the formation rate of ZHS during battery cycling is fast enough to form a denser and more stable SEI, which not only inhibits corrosion, but also provides a fast Zn^{2+} diffusion channel and reduces the charge transfer impedance. However, this resolution is intricate and involves a trade-off; On one hand, the formation of ZHS comes at the cost of irreversible depletion of Zn^{2+} concentration, on the other hand, the heightened pH increases the formation of ZnO, $Zn(OH)_2$ byproducts as well as the risk of battery failure.

In summary, acid-base pH modifiers emerge as influential agents in regulating the initial pH of the electrolyte, thereby have an impact on issues such as the energy storage mechanism of the electrodes, ion kinetic processes, formation of HER and ZHS, and ultimately influence the electrochemical performance of AZIBs. The determination of this pH value necessitates careful consideration not only of the energy storage mechanisms and ion kinetic processes at the characteristic pH of the electrode but also of the influence of side reactions such as HER, ZHS formation, and anodic dissolution on the cycling stability of ZIBs in extreme pH environments.

3.1.2. *Buffer solution*

A buffer solution is a solution capable of resisting changes in pH, thereby maintaining the system's pH at a relatively constant level. This solution type has witnessed significant development in battery applications in recent years. The pH value of a buffer solution depends on the Henderson-Hasselbalch formula (Eq. (15)), i.e., it is determined by the pKa value inherent to the buffer solution as a proton donor (e.g., a weak acid in a weak acid and its conjugate base) as well as by the buffer ratio (the ratio of the concentrations of the buffer pairs). The buffering capacity is determined by the total concentration of the buffer pair and the degree of deviation between the pH value of the buffer solution and the pKa value of the proton donor in the buffer pair. Therefore, it is important to select suitable buffer solutions and appropriate concentration for different applications. At present, buffer solutions applied to AZIBs can be mainly categorized into acetate-based buffer solutions and phosphate-based buffer solutions, such as acetic acid, ammonium acetate and ammonium dihydrogen phosphate.

$$\mathrm{pH} = \mathrm{pk_a(HB)} - \lg\frac{c_{\mathrm{HB}}}{c_{\mathrm{B}}} \tag{15}$$

Han et al. used ammonium acetate (NH_4OAc) as a buffer-like additive to regulate the pH of 2 M $ZnSO_4$, further inhibiting corrosion, HER, and the formation of dendrites [90]. Firstly, the OAC^- in NH_4OAc forms $HOAc/OAc^-$acid-base buffer pairs in the electrolyte to modulate and stabilize the electrolyte pH to around 5.31. Under these conditions (pH=4.11→5.14), the proton-stimulated side reactions (HER and corrosion) are significantly suppressed, while the OH^--directed inert passivation property is difficult to be formed. Furthermore, NH_4^+ serving as an inert cation could homogenize the deposition process of zinc ions and inhibit dendrites formation through the electrostatic shielding effect. Consequently, when monitoring the Zn deposition morphology at a high current density of 10 mA cm^{-2}, was found that the deposits on the surface of Zn anode in the pure electrolyte were uneven and loose, accompanied by the formation of ZHS passivation layer and dendrites, whereas the surface of the Zn electrode was uniform and stable under the regulation of NH_4OAc. In addition to this, the additive had good compatibility with other electrolyte components ($Zn(OTF)_2$, $Zn(OAC)_2$, $ZnCl_2$) as well as the cathode material $NH_4V_4O_{10}$. The pH stabilisation and NH_4^+ established a dissolution equilibrium that suppressed the dissolution of the cathode effectively, avoiding irreversible loss of the active material during the cycling process. Lin et al. similarly investigated NH_4OAc as a buffer based additive (Fig. 4c) [91]. In situ pH monitoring revealed that NH_4OAc had a good pH buffering ability both at low current density (Fig. 4d), high current density, and in low temperatures (−10 °C), which enabled the electrolyte with NH_4OAc to work in harsh operating environments, which greatly improved the low temperature resistance of the electrolyte. In addition to the use of OAc^-, it is also possible to use HOAc directly as a buffer.

In addition to acetate-based buffer solutions, phosphate-based buffer solutions have also been used in AZIBs. Zhang et al. used ammonium NHP additives to stabilize the pH at around 2.8, effectively inhibiting side reactions and dendrite formation (Fig. 4e) [84]. Compared to acetate-based buffer solutions, phosphoric acid undergoes more dissociation processes and has more buffer pairs, such as $(H_2PO_4)^-/(HPO_4)^{2-}$ and $H_3PO_4/(H_2PO_4)^-$, corresponding to pKa values of 7.2 and 2.1, respectively. This implies a broader pH buffer range and, given that the buffering effect depends on the deviation of pKa from the pH value, phosphate-based buffer solution has a better pH buffering effect compared to the acetate-based solution at a specific pH value. (Fig. 4f). In addition, unlike the electrostatic shielding effect of NH_4^+ described in the previous section, it can also form an NH_4^+/NH_3—H_2O buffer pair to stabilize the pH value. Electrolyte pH modulation is equally important in combination with other strategies, Zhao et al. added a small amount of HOAc and organic tetramethylene sulfone (TMS) into $Zn(OTF)_2$ to inhibit HER [92]. The mechanism of the pH buffering of HOAc is similar to that of OAc-, which also buffers the pH by forming an HOAc/OAc-acid-base buffer pair in the electrolyte, resulting in a final pH at 1.6. TMS can also act as a reinforcement of the hydrogen bonding network. Through MD simulations of different electrolytes (Fig. 4g), it was found that in $Zn(OTF)_2$, Zn^{2+} is usually surrounded by H_2O and OTF^- at the first and second coordination shells (Fig. 4h). Upon the introduction of TMS, however, the TMS competes with H_2O at the first and second solvation shells, enabling fewer water molecules to coordinate with Zn^{2+} (Fig. 4i), thereby reducing the activity of H_2O. Simultaneously, part of the TMS would act as a co-solvent, enabling more OTF^- to coordinate with Zn^{2+}, constructing a stronger hydrogen-bonding network between H_2O—H_2O and OTF-H_2O, and inhibiting the HER. As a result, under the joint modulation effect of HOAc and TMS, the pH of $Zn(OTF)_2$ was reduced and stabilized at 1.6, inhibiting the production of the flocculent passivate $Zn_x(OTF)_y(OH)_{2-x-y}{\cdot}nH_2O$. It is essential to clarify that OAc^- and HOAc are not themselves buffer solutions, and only become active when they combine with H^+ and OH^- in electrolyte to form $HOAc/OAc^-$ buffer pairs. Furthermore, although both HOAc and OAc^- can be used as electrolyte additives to form a buffer solution, they have different effects in adjusting the pH value; HOAc as a weak acid combines with OH^- to decrease the pH value, while OAc^- combines with H^+ as a conjugate base to increase the pH value. Importantly, while both HOAc and TMS have the effect of

regulating electrolyte pH, the buffer HOAc can directly stabilize the electrolyte pH by regulating the concentration of H^+/OH^-, which is more effective than TMS in avoiding a unidirectional rise in pH by inhibiting HER. However, it is crucial to note that HER is only one of the challenges faced by AZIBs. Therefore, the combined pH modulation strategy using HOAc/TMS are more effective than using only a single buffer solution.

3.1.3. *Nitrogen-containing heterocyclic organics*

Unlike buffer solutions that utilize the interconversion of buffer pairs to regulate the pH value of the electrolyte, nitrogen-containing heterocyclic organic additives mainly rely on the coordination/de-coordination of the N atom on the molecule structure with H^+ to dynamically regulate the interfacial pH. The organic molecules also tend to preferentially adsorb on the electrode due to the strong adsorption energy, occupying the electric charge double layer (EDL), thus inhibiting the two-dimensional transport of Zn^{2+}, and inducing homogeneous deposition.

Zhang et al. introduced a real-time dynamic strategy for pH buffering at the anode/electrolyte interface, employing N-methylimidazole (NMI) additives [93]. This innovative approach prevents the accumulation of by-products by efficiently eliminating excess OH^-. Illustrated in Fig. 5a, it is revealed that the interfacial absorbing layer, composed of $NMI/NMIH^+$, functions as an ion pump. This pump continuously supplies protons to the interface, effectively inhibiting the formation of ZHS. Results revealed that the Gibbs free energy (ΔG) for the "NMIH–NMI" transition state was close to 0 kJ mol^{-1}, indicating rapid proton transport within NMI molecules (Fig. 5b). Additionally, MD calculations showed a low diffusion coefficient of $NMIH^+$ at the interface (0.031×10^{-5} cm^2 s^{-1}) (Fig. 5c), suggesting challenges in subsequent adsorption–desorption processes. Unlike buffer solutions, the efficacy of organic compounds in pH modulation relies on the proton transport network. In-situ pH measurements within the diffusion layer were conducted using a scanning electrochemical microscope with a ternary pH ultramicroelectrode (UME) (Fig. 5d,e). Results indicated the effectiveness of both the bulk phase and the NMI diffusion layer in stabilizing pH (Fig. 5f). $NMIH^+$ at the interface played a crucial role in reducing crystal radius through electrostatic interactions, promoting

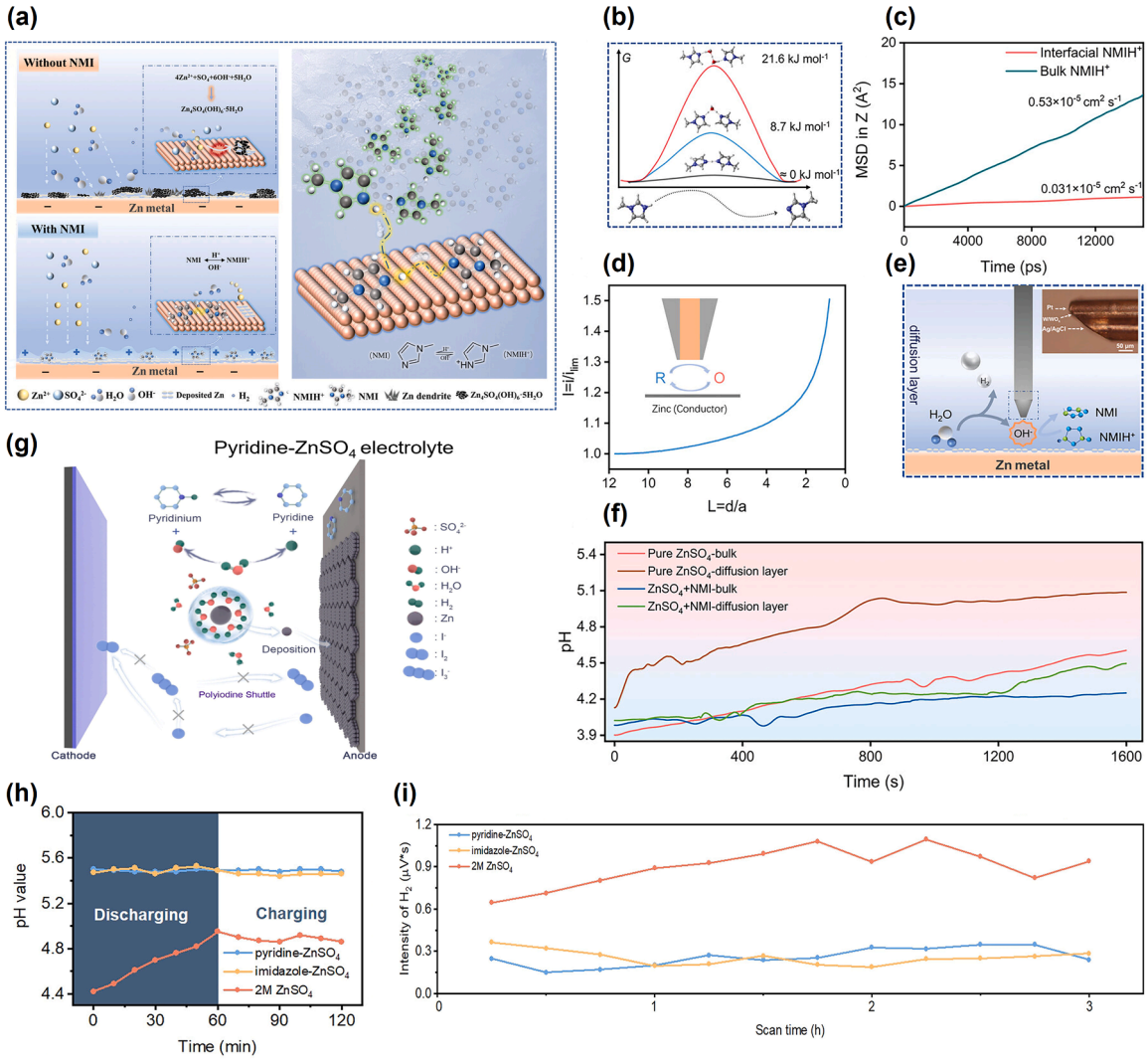

Fig. 5. Regulating electrolyte pH with nitrogen-containing heterocyclic organics. (a) Schematic illustrations of the deposition behavior of Zn anode in $ZnSO_4$ electrolyte with/without NMI additive. (b) Activation Gibbs free energy of different proton-transport processes obtained by quantum chemistry calculation. (c) Diffusion coefficients of $NMIH^+$ in bulk and interface simulated by MD. (d) Approach curve of Pt probe above Zn substrate (inset is a diagram of positive feedback). (e) Diagram of UME detecting pH changes (inset is a microscopy image of pH UME). (f) Measured pH–time curves for bulk phase and diffusion layer in $ZnSO_4$ electrolyte with/without NMI additive. Reprinted with permission from Ref. [94]. Copyright 2023 Willey-VCH. (g) Schematic for mechanism for $Zn-I_2$ full battery in pyridine-$ZnSO_4$ electrolyte. (h) Real-time electrolyte pH near Zn anode during discharge and charge at a current density of 1 mA cm^{-2} and (i) corresponding H_2 release. Reprinted with permission from Ref. [21]. Copyright 2023 The Authors. Published by Willey-VCH.

homogeneous Zn deposition. The uninterrupted proton transport network by NMI/NMH$^+$accelerated MnO_2/Mn^{2+} dissolution/deposition kinetics, enhancing AZIBs discharge capacity and cycling stability. Elsewhere, Lyu et al. utilized another N-containing organic pyridine as a buffer to stabilize pH at the electrode/electrolyte interface (Fig. 5g) [17]. The lone pair on the N atom of pyridine formed a hydrogen bond with H^+, dynamically regulating pH, resulting in electrolyte pH stabilizing at 5.5 during charging and discharging (Fig. 5h). This near-neutral pH reduced the HER tendency at the metal anode interface (Fig. 5i), suppressing polyiodide compound dissolution and minimizing the shuttle effect during cycling.

3.1.4. Electrolyte decoupling

Alkaline ZIBs conventionally operate in an alkaline environment, and although this is favorable for the stability of the Zn metal anode, poorly reversible intermediates such as $Mn(OH)_2$, Mn_2O_3, and Mn_3O_4 are formed at cathode, which restricts the operating voltage and rechargeability of alkaline zinc-based batteries. These factors collectively inhibit the electrochemical performance of the cathode.

AZIBs use a neutral or slightly acidic electrolyte, which greatly enhances the insertion/extraction ability of cations (H^+, Zn^{2+}) at cathode and exhibits enhanced reversibility, however, the redox reaction of cathode, such as MnO_2, limited to Mn^{4+}/Mn^{3+}, and unable to achieve the two-electron reaction of Mn^{4+}/Mn^{2+}, thereby showing limited discharge capacity. At low pH operating environment, although favorable to the capacity and redox potential of the cathode MnO_2, will introduce serious side reactions at zinc anode, such as HER and corrosion, thus limiting the stability and practicality of the full cell. These examples demonstrate that in general the cathode is suitable for acidic environments but the zinc metal anode is suitable for alkaline electrolyte. Hence, decoupling the cathode and anode by situating them in acidic and alkaline environments respectively, can enhance their redox potentials while expanding the ESW. This approach holds promise for greatly improving the operating voltage and reversible capacity of the battery. Liu et al. proposed an electrolyte decoupled battery system (Fig. 6a) [74]. Decoupling the electrolyte into strongly acidic and strongly basic with ion-selective membranes allowed the MnO_2 cathode and Zn anode to operate in strongly acidic and strongly basic electrolytes, respectively, achieving high voltages and high energy densities. The effect of anion-exchange and cation-exchange membranes on the cathode and anode sides is intended to ensure ion-transport channels while preventing, to some extent, the occurrence of neutralization reactions by direct contact between acidic and alkaline solutions. Unlike the electrolyte pH decoupling system in which the cathode and anode are placed in strong acids and bases respectively, Dai et al. decoupled the pH of the same weak acid electrolyte (3 M $Zn(OTF)_2$) by means of an ion exchange membrane (Fig. 6b) [95]. During the cycling of the battery, the ion exchange membrane acts as a proton pump that continuously delivers H^+ to the cathode to lower the pH of the electrolyte on the cathode side to 3.8, which enhances the proton dynamics of the vanadium$^-$based cathode as well as the proton energy storage. On the anode side, the H^+ is pumped away by the ion exchange membrane proton pump to increase the pH to 4.4. The higher pH allows the anode side to form a more stable and dense passivation layer.

Zhong et al. proposed a three-phase electrolyte decoupling system (Fig. 6c) [77]. The acidic solution consisted of sulfuric acid and manganese sulfate, while the alkaline solution consisted of potassium hydroxide, zinc oxide, and trace amounts of vanillin. An anion-exchange membrane and a cation-exchange membrane were placed on the cathode and anode sides, respectively, to generate a central chamber containing a neutral K_2SO_4 electrolyte. The introduction of the central chamber containing the neutral solution further slowed down the neutralization reaction between the acidic and alkaline solutions. Due to the distinctive design of the decoupled battery system, the full battery had a high discharge plateau of ~2.71 V at a current density of 0.1 A g^{-1}, as well as a specific capacity of 616 mAh g^{-1}, which is almost 100 % of

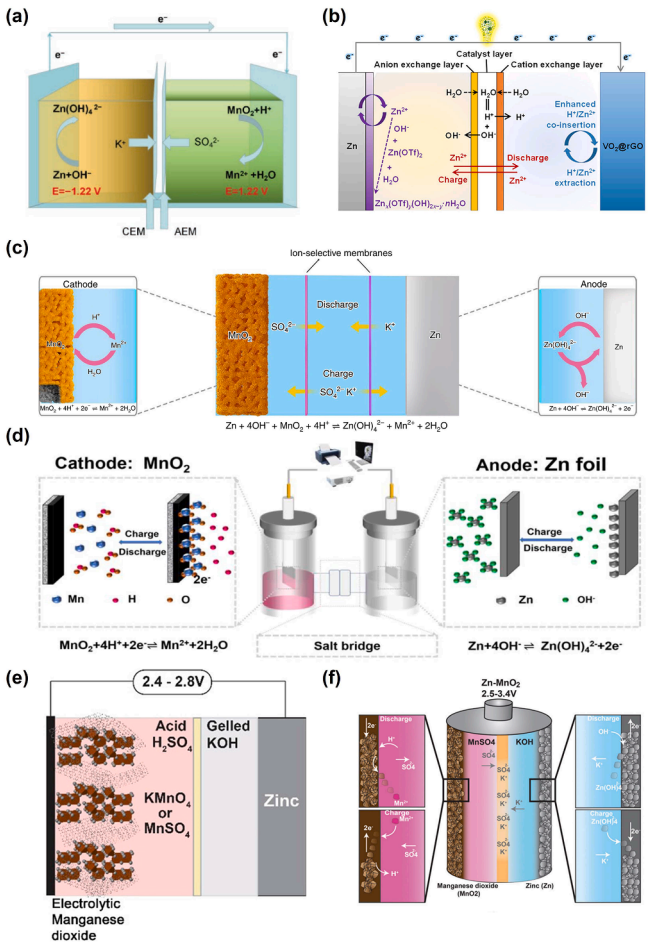

Fig. 6. Regulating electrolyte pH with electrolyte pH decoupling. (a) Electrolyte pH decoupling system with ion exchange membrane. Reprinted with permission from Ref. [92]. Copyright 2020 Willey-VCH.. (b) Single electrolyte pH decoupling system Reprinted with permission from Ref. [96]. Copyright 2021 American Chemical Society. (c) Three-phase electrolyte pH decoupling system. Reprinted with permission from Ref. [22]. Copyright 2020 The Authors. Licensed exclusively to Springer Nature Limited. (d) Electrolyte pH decoupling system with salt bridge. Reprinted with permission from Ref. [97]. Copyright 2022 Elsevier. (e) Membrane-free gel electrolyte pH decoupling system. Reprinted with permission from Ref. [85]. Copyright 2019 American Chemical Society. (f) Electrolyte pH decoupling system with buffer solution gel interlayer. Reprinted with permission from Ref. [84]. Copyright 2014 Royal Society of Chemistry.

the theoretical capacity. Although this cell decoupling system design relying on ion-exchange membranes greatly enhances the operating voltage and reversible capacity of the AZIBs, the higher cost and shorter lifetime of ion-selective membranes limit the development of such cell systems.

Xu et al. similarly developed this three-phase decoupling system (Fig. 6d), but instead of using an ion exchange membrane they used a salt bridge (gel) to remove or minimize the liquid junction potential at the contact of the two electrolytes, which can avoid the direct redox reaction between the two teams of redox pairs [88]. Yadav et al. first reported the design of batteries with 2.45 V and 2.8 V based on an electrolyte decoupling system with ion-selective membrane-free system (Fig. 6e) [79]. In this system, the voltage depended on the use of acidic electrolyte ($KMnO_4$ or $MnSO_4$) on the cathode side and a gelled alkaline electrolyte on the anode side, successfully mitigating the neutralization reaction between the acidic and alkaline electrolyte without the need for costly ion-selective membranes. Instead, a conventional glass fiber separator was directly used, reducing the design and manufacturing cost

of the battery system. However, the relatively high pH of the electrolyte at the cathode still does not trigger the two-electron redox reaction of the cathode MnO_2. The reason for not using a strong acidic cathode electrolyte is mainly that a single gel layer still has a limited effect on the inhibition of the neutralization reaction of the acidic and alkaline electrolytes, and thus cannot ensure the stability of the pH values at both sides during long-term cycling.

Subsequently, Yadav et al. developed a gel-less, film-free electrolyte decoupled system (Fig. 6f), achieving a higher capacity (617 mAh g^{-1}) [78]. Separating the MnO_2 cathode and Zn anode with a gelatinized buffer intermediate layer so that they can operate in different electrolyte environments. Unlike the previously described decoupling system using ion exchange membranes and a single gel layer, this battery system relies on a highly crosslinked poly(potassium acrylate) hydrogel buffer polymer interlayer embedded with an acetic acid buffer solution to isolate both acidic and alkaline solutions and to ensure a stable pH environment for the electrolyte in all parts of the battery system. It was demonstrated that the pH of the Zn/MnO_2 battery changed gently after more than 100 h of cycling, both in the alkaline electrolyte (pH ≈ 9), the acidic electrolyte (pH ≈ 1), and the buffer interlayer (pH ≈ 5).

3.2. Separator modification

The importance of the separator is often overlooked in batteries, typically it serves to provide sufficient wettability and ionic conductivity while avoiding the direct physical contact between the cathode and

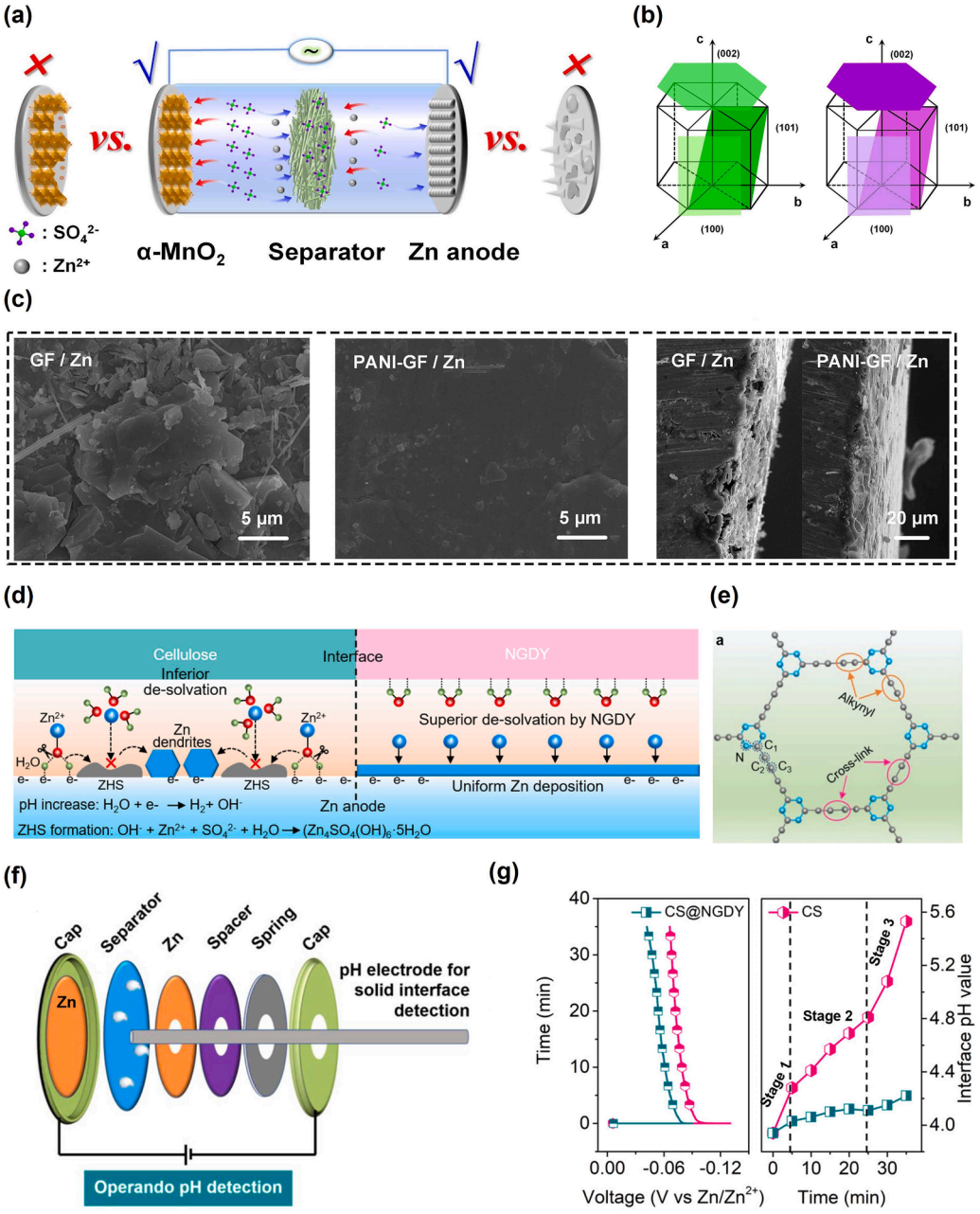

Fig. 7. Adjusting electrolyte pH with membrane modification. (a) Working mechanisms of the Zn|PANI-GF|MnO_2 cells. (b) Color-coded crystal orientation projection for GF and PANI-GF. (c) Surface and cross-sectional scanning electron microscope (SEM) images of Zn electrode for both cells after cycling. Reprinted with permission from Ref. [23]. Copyright 2023 Elsevier. (d) Schematic diagram demonstrating the NGDY-assisted stabilization of interface pH and suppressions of Zn dendrites. (e) Synthesis and characterization of NGDY interface. (f) The home-made operando pH detection configuration. (g) Real-time interface pH change at the Zn anode region at the current density of 5 mA cm^{-2}. Reprinted with permission from Ref. [20]. Copyright 2021 Willey-VCH.

anode, avoiding the short circuit caused by, for example, Zn dendrite growth [86,87,89,98]. Recently a series of novel glass fiber (GF) separators with abundant polar groups (amino, carbonyl, and triazine) have been designed in recent years to significantly improve the reversibility of Zn deposition/stripping by inhibiting dendrites formation and reducing side reactions [94,96,97,99]. However, most of the current separator modifications still focus on addressing the issues at anode, with few reports of separators capable of stabilizing both the cathode and anode, and even fewer linking them to pH regulation. Hence, it is worth giving due attention to functional separators with special functional groups, such as —NH_2, —C═O. The functional groups on separator can coordinate with Zn^{2+} ions and accelerate their desolvation process. Consequently, electrons can directly transfer from Zn^{2+} ions, weakening of O—H bond and thus reducing HER and stabilizing interface pH value for both sides.

Polyaniline (PANI), as a conductive polymer, has been widely used in batteries [100–104] for example by compounding with cathode materials to increase the conductivity or improving the hydrophilicity and zincophilicity of the metal interface, which results in higher discharge capacity and more stable cycling performance [105–107]. However, so far, polyaniline has only been able to solve the problems faced by a single electrode. Zhao et al. improved both anode and cathode cycle performance by in situ synthesis of a polyaniline-functionalized glass fiber separator (PANI-GF) (Fig. 7a) [108]. PANI-GF demonstrated the capability to simultaneously stabilize the pH value of the cathode/electrolyte and anode/electrolyte interfaces through a protonation process that inhibited the occurrence of side reactions at the anode interface as well as the dissolution of the cathode. The inhibitory effect of PANI-GF on the HER was attributed to its stronger Zn trapping capacity and higher free energy of hydrogen precipitation on the (002) crystal planes (Fig. 7b). As a result of these synergistic effects, the Zn electrode based on PANI-GF after cycling exhibited a neat and smooth surface free of dendrites (Fig. 7c).

Yang et al. constructed N-modified graphdiyne (NGDY) interface on a cellulose separator to inhibit the formation of interfacial dendrites (Fig. 7d,e) [16]. Through real-time operando monitoring of the pH changes at the Zn metal interface (Fig. 7f), it was observed this NGDY-based interface successfully stabilized the pH in the range of 3.94 to 4.22 (Fig. 7g). This pH stabilization was attributed to the accelerated NGI-mediated de-solvation of the hydrated Zn ion, facilitating the direct electron transfer from the metal anode to Zn^{2+} rather than to the coordinated H_2O, thus avoiding the breakage of the O—H bond, suppressing HER and its resultant increase in pH.

3.3. Artificial interface protective layers

A common approach to protect and stabilize both electrodes involves constructing a series of AIPLs on their surfaces. For example, the construction of nanoporous AIPLs with an ionic confinement effect aim to inhibit dendrites by homogenizing the Zn flux [45,109–112]. Beyond the ionic confinement effect, some AIPLs with abundant zincophilic sites, including metal-organic frameworks (MOFs), $Ca_5(PO_4)_3(OH)$, $ZnSnO_3$ and some organic compounds with specific functional groups (such as carbonyl [—C═O] and amino [—NH_2] groups) [113–117], and nitrogen-doped graphene [16], have been proposed to impede the lateral migration of Zn^{2+} along the electrode-electrolyte interface and provide more nucleation sites, thus inducing uniform Zn deposition.

However, direct contact between the electrolyte and the metal anode cannot be completely avoided for these loose AIPLs, allowing for the occurrence of HER and corrosion reactions. To address this, dense SEI layers, such as ZnS, ZnF_2, $Zn_3(PO_4)_2$, ZnSe, and polydopamine (PDA) can be constructed in-situ on the Zn electrode, blocking the direct contact between the electrolyte and the surface of the zinc metal, thus inhibiting the occurrence of undesirable side reactions [118–124]. However, the high-energy barriers of these dense protective layers will hinder the diffusion of Zn^{2+}, leading to higher charge transfer impedance and polarization, which affects the electrochemical performance of AZIBs. These AIPLs also usually lack mechanical elasticity, so irreversible structural fractures will inevitably occur during cycling, which will make the protection less effective. Therefore, various flexible organic polymer AIPLs have been proposed as alternatives.

In summary, people have successfully inhibited dendrite formation, HER and corrosion reactions at the zinc metal surface by AIPLs. Considering that the pH value affects the Zn flux and leads to the formation of dendrites, and further, HER, passivation, and corrosion of Zn also have a certain relationship with the pH value, therefore, a number of AIPLs with the function of pH modulation have been put forward in recent years. These can be broadly categorized into two main groups: inorganic and organic materials. Certain inorganic materials are capable of self-dissolution within a specific pH range, functioning similarly to electrolyte additives, thus enabling pH regulation. While organic substances can effectively regulate the localized concentration of H^+ and OH^- at the anode interface by manipulating the Lewis acid-base interactions, thus reducing HER and corrosion, and mitigating ZHS formation at the metal anode surface.

3.3.1. Inorganic materials

Some inorganic materials, such as ZnS,ZnF_2, $Zn_3(PO_4)_2$ and ZnSe, are frequently employed as AIPLs due to their higher thermal stability, chemical durability, and enhanced mechanical strength for safeguarding electrode materials [119–122,125]. Considering the significance of pH values in AZIBs, recently developed inorganic AIPLs play a crucial role in regulating pH values [113,116]. These inorganic materials not only enhance the HER barrier by physically isolating the zinc anode from direct contact with the electrolyte or through specific atomic interactions to modulate the electrolyte's pH, but they also regulate the electrolyte's pH by undergoing self-dissolution within a certain pH range, akin to electrolyte additives.

Qi et al. achieved pH modulation at the electrode/electrolyte interface by constructing an enamel-like nanohydroxyapatite (E-nhap) layer on the surface of the Zn [116]. This effectively suppressed the HER, corrosion and passivation of the Zn anode (Fig. 8a). Nanohydroxyapatite $Ca_5(PO_4)_3(OH)$ is a slightly alkaline material, and the soluble E-hap layer released the weakly alkaline anion PO_4^{3-} in weakly acidic environments, which leads to the spontaneous formation of a phosphate-based buffer solution with a buffer pair of $H_2PO_4^-/HPO_4^{2-}$ in the electrolyte, regulating the concentration of H^+/OH^-, thus stabilizing the pH in a mild environment (pH ≈ 5.1). Here, the initial pH of the electrolyte rises due to the addition of PO_4^{3-}, which reduces the tendency of corrosion, HER, in addition to the pH buffering effect brought about by the buffer solution so that the pH is always lower than the ZHS formation threshold (pH>5.47), which in turn inhibits the production of passivation products. E-nhap facilitated ion exchange between Ca^{2+} and Zn^{2+} while the remaining crystal structure unchanged, thus providing sufficient and uniform Zn-philic sites and realizing dendrite-free Zn deposition. Ling et al. proposed a multiscale (electron-crystal-geometry) structural design concept to accurately construct hollow amorphous $ZnSnO_3$ (HZTO) AIPLs on the Zn anode surface (Fig. 8b) [113]. HZTO was designed to suppress HER and inhibit the increase of pH at the anode/electrolyte interface. The suppression of HER was mainly attributed to the introduction of the Sn, which enhances interactions between O and H atoms, thus increasing the HER energy barrier.

As a result, the pH of the HZTO@Zn/electrolyte interface was consistently maintained at around 3.13, both during the operation of the Zn-symmetric cell and during the stationary process in the strong acid solution (Fig. 8c,d). In addition, the abundant Zn-friendly sites, excellent conductivity, and thin-shelled hollow structure of HZTO favored uniform Zn nucleation as well as fast Zn^{2+} diffusion kinetics. DFT was employed to better understand the mechanism of HZTO inhibiting HER. As shown in Fig. 8e, the adsorption Gibbs free energy ($\triangle G_H$) of HZTO (−2.07 eV) for hydrogen is lower than that of ZnO (−0.23 eV) and Zn (0.5 eV), indicating enhanced hydrogen adsorption by HZTO, thereby

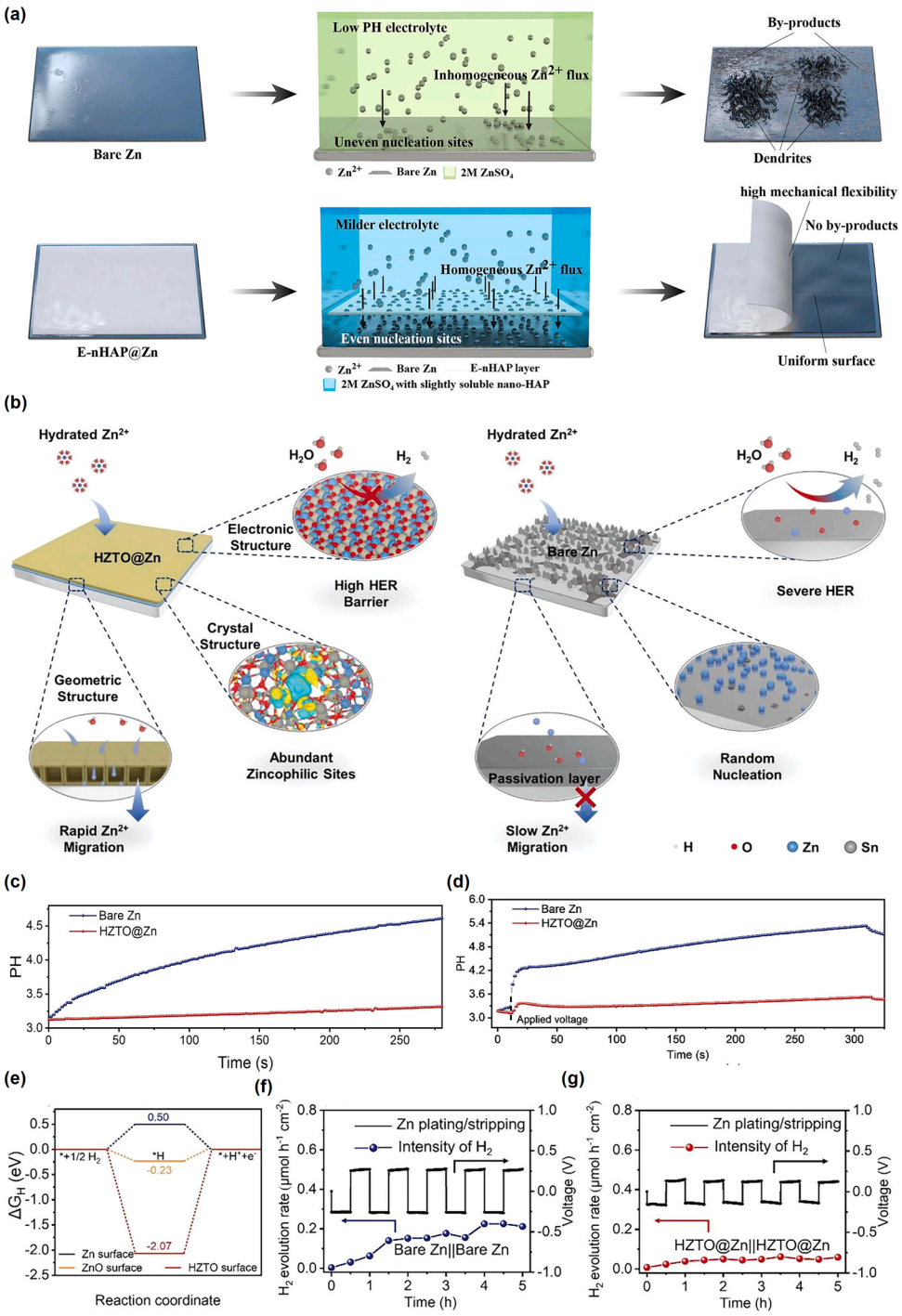

Fig. 8. Regulating electrolyte pH with inorganic AIPLs. (a) Comparison of the Zn deposition mechanisms between E-nHAP@Zn and bare Zn surfaces. Reprinted with permission from Ref. [121]. Copyright 2022 American Chemical Society. (b) Schematic illustrations depicting the Zn anode's deposition behavior with/without AIPLs of HZTO. In situ pH changes were monitored in the interface region of the Zn anode under static exposure in diluted H_2SO_4 (c) and during cycling in $ZnSO_4$ at a current density of 5 mA cm^{-2} (d). (e) Gibbs free energy diagram for hydrogen evolution on the surfaces of Zn (101), ZnO and HZTO. In situ measurement of hydrogen evolution rate for (f) the bare Zn||Zn battery and (g) HZTO@Zn||HZTO@Zn battery at 5 mA cm^{-2} during the discharge/charge process. Reprinted with permission from Ref. [119]. Copyright 2023 Willey-VCH.

increasing the energy barrier of HER. Additionally, the hydrogen generation rate (R_H) in symmetrical cells with and without AIPLs was quantitatively detected by gas chromatography. The results demonstrated that for the pure Zn anode the HER rate increases rapidly due to the enlarged active Zn metal area caused by partial oxidation during cycling and uneven deposition of Zn^{2+} (Fig. 8f). In contrast, HZTO@Zn inhibits HER by impeding the diffusion of Zn^{2+} through the corrosion passivation layer (Fig. 8g).

3.3.2. *Organic materials*

Organic AIPLs possess enough polar groups to establish good interfacial contact with the Zn electrode compared to inorganic materials, so they can provide a more uniform Zn^{2+} flux. More importantly, organic materials featuring diverse functional groups (—NH_2, —OH, —SO_3H,

and —COOH) can effectively regulate the localized concentration of H^+ and OH^- at the interface of a modified metal anode by manipulating the Lewis acid-base interactions. This, in turn, inhibits HER and corrosion, while also preventing the formation of ZHS at the anode side.

Ke et al. constructed imidazolium polymer ionic liquids by in-situ polymerization on the zinc metal surface (1-carboxymethyl-3-vinyl-imidazolium bromide monomer, CVBr), forming a crosslinked acryl-amide (AM) interfacial layer (Zn@CVBr|AM) to inhibit HER and the formation of ZHS (Fig. 9a,b) [117]. The uniformly coated CVBr|AM layer on the Zn surface led to a more stable pH change at the metal/-electrolyte interface, maintaining the pH at around 3.54 (Fig. 9c). The lower pH value suppressed the formation of ZHS, as evidenced by XRD patterns (Fig. 9d). The stabilization of the pH value was attributed to the fact that the N atoms of imidazole complex with Zn^{2+} and H^+ in the electrolyte and inhibited HERs by impeding the transfer of the reactive H_2O. In addition, the CVBr|AM layer had the effect of enhancing ionic conductivity and homogenizing Zn deposition. The evolution of the Zn@CVBr|AM gel coatings showed no H_2 accumulation on the anode surface, indicating effective protection. This observation aligned with the morphology observed using SEM and the atomic force microscope (AFM) (Fig. 9e-i). Li et al. developed a series of AIPLs based on UiO-66MOFs with different functional groups (—NH_2, —OH, —SO_3H,

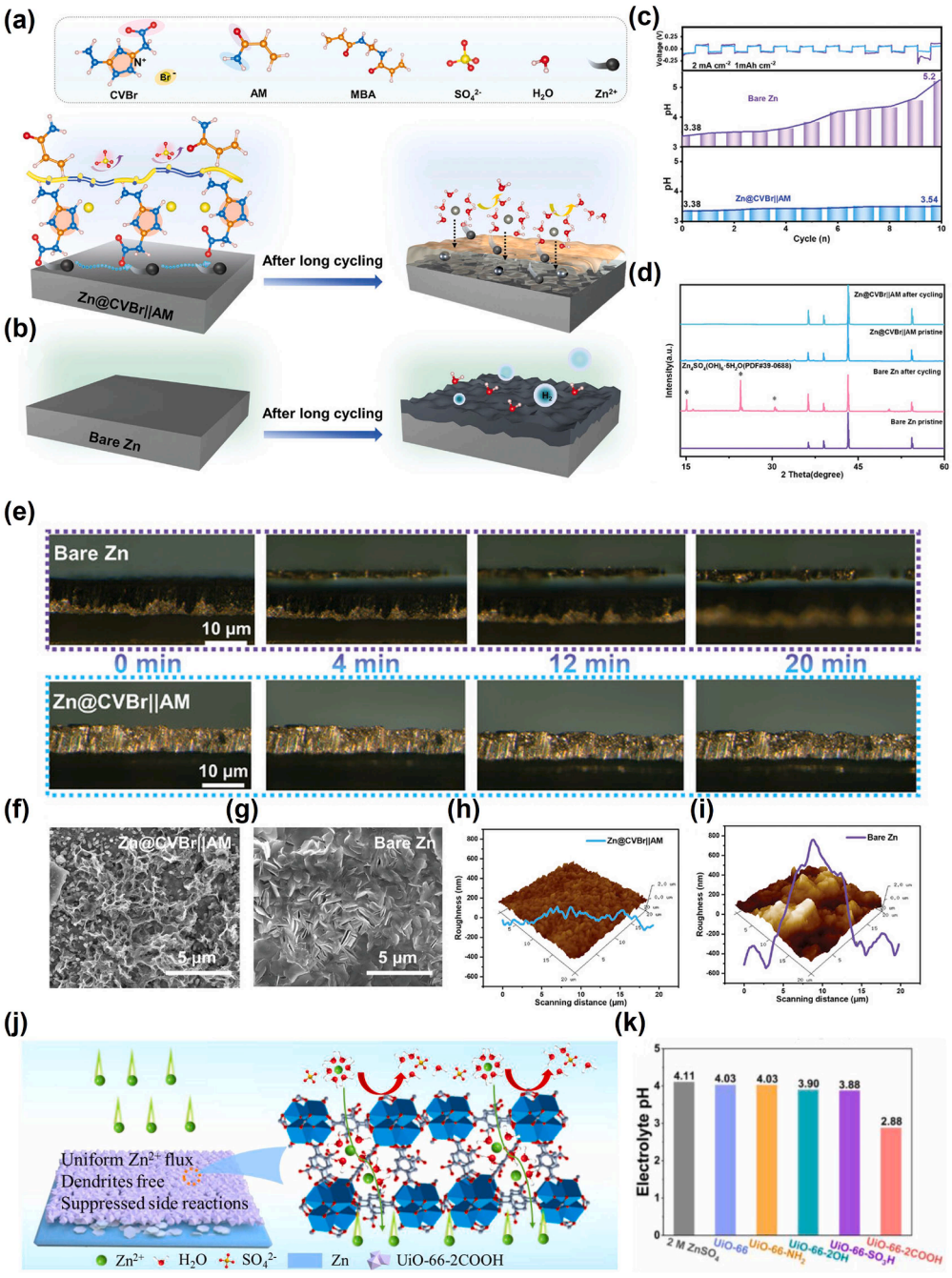

Fig. 9. Schematic illustration of PolyCVBr||AM and Zn^{2+} deposition processes on (a) Zn@CVBr||AM and (b) bare Zn. (c) In situ pH changes within 10 cycles and corresponding galvanostatic curve. (d) In situ XRD patterns of bare Zn and Zn@CVBr||AM before and after 200h cycling. (e) In situ optical pictures of Zn deposition at different minutes. SEM images of (f) Zn@CVBr||AM and (g) bare Zn after 200 h cycling. 3D confocal AFM and the relative roughness curve of (h) Zn@CVBr||AM and (i) bare Zn. Reprinted with permission from Ref. [122]. Copyright 2023 Willey-VCH. (j) Schematic diagram of Zn deposition on bare Zn and Zn@UiO-66-2COOH. (k) The pH values of 2 M $ZnSO_4$ solution with or without UiO-66-X powders. Reprinted with permission from Ref. [24]. Copyright 2023 Elsevier.

and —COOH) [115]. These AIPLs aimed to regulate the localized pH value of the anode interface and inhibit the formation of ZHS by manipulating the Lewis acid-base interactions within the MOFs at the molecular level (Fig. 9j). In addition, the AIPLs have the effect of optimizing Zn^{2+} diffusion and deposition behavior and accelerating desolvation process. The results showed that UiO-66-2COOH was able to significantly reduce the electrolyte pH (pH=4.11→2.88) compared to MOFs with other functional groups, which was attributed to the —COOH groups. The acidic—COOH groups in UiO-66-2COOH are effective in releasing protons to regulate the local pH environment at the anode interface (Fig. 9k). This approach differs from acid-base pH regulators (e.g., H_2SO_4), which use neutralization reactions for global pH regulation of the electrolyte. The focus here is on regulating the local pH to inhibit the formation of passivating ZHS.

4. Conclusion and perspectives

In summary, the pH value of aqueous electrolytes is closely linked to the electrochemical performance of AZIBs, including the reversibility of metallic zinc anode and the charge/discharge mechanism of cathodes. Therefore, to maximize the potential of AZIBs it is essential that the optimal electrolyte pH environment for both the cathode and anode is quickly established and maintained throughout the full cycling life of the cell.

Since most of the issues on the metal anode, including HER, corrosion, passivation, and dendrites, are closely related to electrolyte pH, pH regulation strategies can solve the problems more fundamentally compared with other strategies to improve the zinc storage performance. Additionally, pH modulation strategies based on electrolyte engineering, separator modification, and AIPLs can be used in concert with other protection strategies to synergistically improve the electrochemical performance of full cell. However, unsuitable pH control strategies and excessive electrolyte additions may bring additional undesired side reactions and thus degrade the electrochemical performance of the battery.

In addition to further optimization of the methods discussed above, we believe that the following research directions related to electrolyte pH regulation should be considered as priorities for future AZIBs stabilization strategies:

(1) When improving the electrolyte environment of different components, most published studies focus on addressing the issues occurring on the metal anode side and a comprehensive understanding of the underlying mechanisms of additives on cathode materials remains insufficient. Although existing literature demonstrated good compatibility of additives with both the anode and cathode, there are still few studies systematically addressing the simultaneous enhancement of the operational environment for each component of AZIBs through electrolyte regulation strategies. Consequently, there is a discernible gap necessitating further investigation, particularly through the adoption of a holistic "whole-cell" approach to comprehensively elucidate the intricacies of the interplay between the anode, cathode, and electrolyte within AZIBs.

(2) According to the control mechanism, HER inhibition strategies are mainly divided into two types: reduction of HER potential and control of H^+ concentration, but neither control mechanism can currently overcome all of the problems of the zinc anode. For example, buffer solutions can stabilize H^+ concentration, thereby inhibiting the pH change of the electrolyte, but it does not directly inhibit the occurrence of HER. Similarly, the strategy of inhibiting HER does not directly participate in the regulation process of H^+ concentration, so the pH regulation effect is limited. At the same time, there are factors that affect the pH value of the electrolyte during battery operation, and this strategy cannot prevent it. Therefore, synergistic stabilization of pH fluctuations and inhibition of HER through paired regulatory mechanisms should become a primary research focus.

(3) Summarizing and comparing the advantages and disadvantages of different buffer systems and choosing the optimal buffer pair. Buffer solutions are typical AZIBs electrolyte additives that suppresses pH changes by regulating H^+ concentration. Current research mainly focuses on acetic acid series, but rarely the phosphoric acid series, and other types of buffer solutions (such as oxalates, tartrates) have yet to be studied widely, despite their promise for AZIBs stabilization. Furthermore, the buffer ratio and total buffer concentration of the buffer solution determine the buffering effect of the buffer solution, but if this concentration is non-ideal buffers may also produce more side reactions, causing the buffer system or the battery to fail, even if excess buffer solution additives can theoretically achieve a better buffering effect. Additionally, environmentally friendly pH regulators should be prioritized, such as some biodegradable substances, to reduce the adverse impact of regulators on the environment, especially in the context of the push for carbon neutrality. Therefore, further systematic research and inter-comparison of the selection and preparation principles of AZIBs battery buffer solutions will be of great importance.

(4) Real-time pH monitoring and feedback control in a real battery environment remains a priority. Literature reports show that when testing the pH changes of electrolyte in real time, two test systems are often used, one is a self-made open beaker battery, and the other is a button battery with holes. Both open test systems are very different from the actual battery environment. Therefore, developing systems to integrate pH sensors into truly representative battery systems will more effectively enable the impact of pH regulation in the electrolyte, enabling the monitoring the pH value in real time and continual feedback control measures. This will provide valuable evidence to inform onward design strategies.

(5) Studies to date have shown that among all regulating strategies, the electrolyte decoupling strategy is the most promising way to regulate electrolyte pH, as it can accommodate the different operating environments of both cathode and anode. However, additional efforts are required to approach the practical application of high-energy-density AZIBs, focusing on cost-effectiveness and achieving excellent cycle stability.

Overall, although the industrialization of aqueous batteries remains a formidable challenge, the current research progress suggests that they hold considerable promise as prospective candidates for future applications. This work summarizes the current research advances on pH regulation and aims to build a robust foundation for the development of scalable and sustainable energy storage technologies.

CRediT authorship contribution statement

Mingqiang Liu: Writing – original draft, Conceptualization. **Peiqingfen Wang:** Writing – review & editing, Writing – original draft, Conceptualization. **Wei Zhang:** Writing – review & editing. **Hongzhen He:** Writing – review & editing, Conceptualization. **Guanjie He:** Writing – review & editing. **Shusheng Xu:** Writing – review & editing. **Lu Yao:** Writing – review & editing, Writing – original draft, Conceptualization. **Thomas S. Miller:** Writing – review & editing, Conceptualization, Supervision, Funding acquisition.

Declaration of competing interest

The authors declare the following financial interests/personal relationships which may be considered as potential competing interests:

T.S. Miller reports financial support was provided by The Faraday Institution. If there are other authors, they declare that they have no

known competing financial interests or personal relationships that could have appeared to influence the work reported in this paper.

Data availability

No data was used for the research described in the article.

Acknowledgements

We would like to thank for the financially supported by a University College London Dean's Prize, China Scholarships Council funding. We also appreciate the support of the U.K. Faraday Institution LiSTAR programme (EP/S003053/1, FIRG014, FIRG058) and for research funding from the National Natural Science Foundation of China (62241406).

References

[1] M. Winter, B. Barnett, K. Xu, Before Li ion batteries, Chem. Rev. 118 (2018) 11433–11456, https://doi.org/10.1021/acs.chemrev.8b00422.
[2] N. Nitta, F. Wu, J.T. Lee, G. Yushin, Li-ion battery materials: present and future, Mater. Today 18 (2015) 252–264, https://doi.org/10.1016/j.mattod.2014.10.040.
[3] T. Liu, X. Zhang, M. Xia, H. Yu, N. Peng, C. Jiang, M. Shui, Y. Xie, T.-F. Yi, J. Shu, Functional cation defects engineering in TiS_2 for high-stability anode, Nano Energy 67 (2020) 104295, https://doi.org/10.1016/j.nanoen.2019.104295.
[4] Z. Xing, C. Huang, Z. Hu, Advances and strategies in electrolyte regulation for aqueous zinc-based batteries, Coord. Chem. Rev. 452 (2022) 214299, https://doi.org/10.1016/j.ccr.2021.214299.
[5] R. Zheng, S. Qian, X. Cheng, H. Yu, N. Peng, T. Liu, J. Zhang, M. Xia, H. Zhu, J. Shu, $FeNb_{11}O_{29}$ nanotubes: superior electrochemical energy storage performance and operating mechanism, Nano Energy 58 (2019) 399–409, https://doi.org/10.1016/j.nanoen.2019.01.065.
[6] Y. He, Y. Cui, W. Shang, Z. Zhao, P. Tan, Insight into potential oscillation behaviors during Zn electrodeposition: mechanism and inspiration for rechargeable Zn batteries, Chem. Eng. J. 438 (2022) 135541, https://doi.org/10.1016/j.cej.2022.135541.
[7] Q. Zhao, Z. Yan, C. Chen, J. Chen, Spinels: controlled preparation, oxygen reduction/evolution reaction application, and beyond, Chem. Rev. 117 (2017) 10121–10211, https://doi.org/10.1021/acs.chemrev.7b00051.
[8] K.L. Ng, B. Amrithraj, G. Azimi, Nonaqueous rechargeable aluminum batteries, Joule 6 (2022) 134–170, https://doi.org/10.1016/j.joule.2021.12.003.
[9] Z. Cheng, B. Zhao, Y. Guo, L. Yu, B. Yuan, W. Hua, Y. Yin, S. Xu, B. Xiao, X. Han, P. Wang, Y. Guo, Mitigating the large-volume phase transition of P2-type cathodes by synergetic effect of multiple ions for improved sodium-ion batteries, Adv. Energy Mater. 12 (2022) 2103461, https://doi.org/10.1002/aenm.202103461.
[10] Z. Liu, L. Qin, X. Cao, J. Zhou, A. Pan, G. Fang, S. Wang, S. Liang, Ion migration and defect effect of electrode materials in multivalent-ion batteries, Prog. Mater. Sci. 125 (2022) 100911, https://doi.org/10.1016/j.pmatsci.2021.100911.
[11] C. Wei, L. Tan, Y. Zhang, B. Xi, S. Xiong, J. Feng, Y. Qian, Highly reversible Mg metal anodes enabled by interfacial liquid metal engineering for high-energy Mg-S batteries, Energy Storage Mater. 48 (2022) 447–457, https://doi.org/10.1016/j.ensm.2022.03.046.
[12] M. Li, Z. Li, X. Wang, J. Meng, X. Liu, B. Wu, C. Han, L. Mai, Comprehensive understanding of the roles of water molecules in aqueous Zn-ion batteries: from electrolytes to electrode materials, Energy Environ. Sci. 14 (2021) 3796–3839, https://doi.org/10.1039/D1EE00030F.
[13] C. Li, A. Shyamsunder, A.G. Hoane, D.M. Long, C.Y. Kwok, P.G. Kotula, K. R. Zavadil, A.A. Gewirth, L.F. Nazar, Highly reversible Zn anode with a practical areal capacity enabled by a sustainable electrolyte and superacid interfacial chemistry, Joule 6 (2022) 1103–1120, https://doi.org/10.1016/j.joule.2022.04.017.
[14] D. Qiu, B. Li, C. Zhao, J. Dang, G. Chen, H. Qiu, H. Miao, A review on zinc electrodes in alkaline electrolyte: current challenges and optimization strategies, Energy Storage Mater. 61 (2023) 102903, https://doi.org/10.1016/j.ensm.2023.102903.
[15] P. Xiao, H. Li, J. Fu, C. Zeng, Y. Zhao, T. Zhai, H. Li, An anticorrosive zinc metal anode with ultra-long cycle life over one year, Energy Environ. Sci. 15 (2022) 1638–1646, https://doi.org/10.1039/D1EE03882F.
[16] Q. Yang, L. Li, T. Hussain, D. Wang, L. Hui, Y. Guo, G. Liang, X. Li, Z. Chen, Z. Huang, Y. Li, Y. Xue, Z. Zuo, J. Qiu, Y. Li, C. Zhi, Stabilizing interface pH by N-modified graphdiyne for dendrite-free and high-rate aqueous Zn-ion batteries, Angew. Chem. Int. Ed. 61 (2022), https://doi.org/10.1002/anie.202112304.
[17] Y. Lyu, J.A. Yuwono, P. Wang, Y. Wang, F. Yang, S. Liu, S. Zhang, B. Wang, K. Davey, J. Mao, Z. Guo, Organic pH buffer for dendrite-free and shuttle-free Zn-I_2 batteries, Angew. Chem. Int. Ed. 62 (2023) e202303011, https://doi.org/10.1002/anie.202303011.
[18] K. Ouyang, S. Chen, W. Ling, M. Cui, Q. Ma, K. Zhang, P. Zhang, Y. Huang, Synergistic modulation of in-situ hybrid interface construction and pH buffering enabled ultra-stable zinc anode at high current density and areal capacity, Angew. Chem. Int. Ed. 62 (2023) e202311988, https://doi.org/10.1002/anie.202311988.
[19] J. Hao, X. Li, X. Zeng, D. Li, J. Mao, Z. Guo, Deeply understanding the Zn anode behaviour and corresponding improvement strategies in different aqueous Zn-based batteries, Energy Environ. Sci. 13 (2020) 3917–3949, https://doi.org/10.1039/d0ee02162h.
[20] S. Debnath, A. Maiti, P. Naskar, A. Banerjee, Rechargeable manganese dioxide−zinc batteries: a review focusing on challenges and optimization strategies under alkaline and mild acidic electrolyte media, ChemNanoMat 8 (2022) e202200261, https://doi.org/10.1002/cnma.202200261.
[21] A.Z. Durena, A short review: comparison of zinc–manganese dioxide batteries with different ph aqueous electrolytes, Batteries 9 (2023) 311, https://doi.org/10.3390/batteries9060311.
[22] J. Ding, Z. Du, L. Gu, B. Li, L. Wang, S. Wang, Y. Gong, S. Yang, Ultrafast Zn^{2+} intercalation and deintercalation in vanadium dioxide, Adv. Mater. 30 (2018) 1800762, https://doi.org/10.1002/adma.201800762.
[23] T. Wang, S. Li, X. Weng, L. Gao, Y. Yan, N. Zhang, X. Qu, L. Jiao, Y. Liu, Ultrafast 3D hybrid-ion transport in porous V_2O_5 cathodes for superior-rate rechargeable aqueous zinc batteries, Adv. Energy Mater. 13 (2023) 2204358, https://doi.org/10.1002/aenm.202204358.
[24] Y. Chen, D. Ma, K. Ouyang, M. Yang, S. Shen, Y. Wang, H. Mi, L. Sun, C. He, P. Zhang, A multifunctional anti-proton electrolyte for high-rate and super-stable aqueous Zn-vanadium oxide battery, Nano-Micro Lett. 14 (2022), https://doi.org/10.1007/s40820-022-00907-4.
[25] X. Zhu, Z. Cao, W. Wang, H. Li, J. Dong, S. Gao, D. Xu, L. Li, J. Shen, M. Ye, Superior-performance aqueous zinc-ion batteries based on the in situ growth of MnO_2 nanosheets on V_2CT_x MXene, ACS Nano 15 (2021) 2971–2983, https://doi.org/10.1021/acsnano.0c09205.
[26] J. Zhao, Z. Xu, Z. Zhou, S. Xi, Y. Xia, Q. Zhang, L. Huang, L. Mei, Y. Jiang, J. Gao, Z. Zeng, C. Tan, A safe flexible self-powered wristband system by integrating defective MnO_2-x nanosheet-based zinc-ion batteries with perovskite solar cells, ACS Nano 15 (2021) 10597–10608, https://doi.org/10.1021/acsnano.1c03341.
[27] D. Zhang, J. Cao, X. Zhang, N. Insin, S. Wang, J. Han, Y. Zhao, J. Qin, Y. Huang, Inhibition of manganese dissolution in Mn_2O_3 cathode with controllable Ni^{2+} incorporation for high-performance zinc ion battery, Adv. Funct. Mater. 31 (2021), https://doi.org/10.1002/adfm.202009412.
[28] M. Chen, J. Chen, W. Zhou, X. Han, Y. Yao, C.-P. Wong, Realizing an all-round hydrogel electrolyte toward environmentally adaptive dendrite-free aqueous Zn-MnO_2 batteries, Adv. Mater. 33 (2021), https://doi.org/10.1002/adma.202007559.
[29] X. Chen, H. Zhang, J.-H. Liu, Y. Gao, X. Cao, C. Zhan, Y. Wang, S. Wang, S.-L. Chou, S.-X. Dou, D. Cao, Vanadium-based cathodes for aqueous zinc-ion batteries: mechanism, design strategies and challenges, Energy Storage Mater. 50 (2022) 21–46, https://doi.org/10.1016/j.ensm.2022.04.040.
[30] H. Liu, L. Jiang, B. Cao, H. Du, H. Lu, Y. Ma, H. Wang, H. Guo, Q. Huang, B. Xu, S. Guo, Van der Waals interaction-driven self-assembly of V_2O_5 nanoplates and mxene for high-performing zinc-ion batteries by suppressing vanadium dissolution, ACS Nano 16 (2022) 14539–14548, https://doi.org/10.1021/acsnano.2c04968.
[31] Y. Zhang, C. Zhao, Z. Li, Y. Wang, L. Yan, J. Ma, Y. Wang, Synergistic co-reaction of Zn^{2+} and H^+ with carbonyl groups towards stable aqueous zinc-organic batteries Br, Energy Storage Mater. 52 (2022) 386–394, https://doi.org/10.1016/j.ensm.2022.08.005.
[32] X. Wu, X. Feng, J. Yuan, X. Yang, H. Shu, C. Yang, Z. Liu, J. Peng, E. Liu, S. Tan, P. Gao, Thiophene functionalized porphyrin complexes as novel bipolar organic cathodes with high energy density and long cycle life, Energy Storage Mater. 46 (2022) 252–258, https://doi.org/10.1016/j.ensm.2022.01.020.
[33] H. Wang, Q. Wu, L. Cheng, G. Zhu, The emerging aqueous zinc-organic battery, Coord. Chem. Rev. 472 (2022), https://doi.org/10.1016/j.ccr.2022.214772.
[34] H. Peng, C. Liu, N. Wang, C. Wang, D. Wang, Y. Li, B. Chen, J. Yang, Y. Qian, Intercalation of organics into layered structures enables superior interface compatibility and fast charge diffusion for dendrite-free Zn anodes, Energy Environ. Sci. 15 (2022) 1682–1693, https://doi.org/10.1039/d1ee03624f.
[35] Z. Li, J. Tan, X. Zhu, S. Xie, H. Fang, M. Ye, J. Shen, High capacity and long-life aqueous zinc-ion battery enabled by improving active sites utilization and protons insertion in polymer cathode, Energy Storage Mater. 51 (2022) 294–305, https://doi.org/10.1016/j.ensm.2022.06.049.
[36] H. Cui, L. Ma, Z. Huang, Z. Chen, C. Zhi, Organic materials-based cathode for zinc ion battery, Smartmat 3 (2022) 565–581, https://doi.org/10.1002/smm2.1110.
[37] Z. Chen, H. Cui, Y. Hou, X. Wang, X. Jin, A. Chen, Q. Yang, D. Wang, Z. Huang, C. Zhi, Anion-chemistry-enabled positive valence conversion to achieve a record-high-voltage organic cathode for zinc batteries, Chemistry 8 (2022) 2204–2216, https://doi.org/10.1016/j.chempr.2022.05.001.
[38] Y. Cao, M. Wang, H. Wang, C. Han, F. Pan, J. Sun, Covalent organic framework for rechargeable batteries: mechanisms and properties of ionic conduction, Adv. Energy Mater. 12 (2022), https://doi.org/10.1002/aenm.202200057.
[39] H. Zhang, J. Peng, L. Li, Y. Zhao, Y. Gao, J. Wang, Y. Cao, S. Dou, S. Chou, Low-cost zinc substitution of iron-based prussian blue analogs as long lifespan cathode materials for fast charging sodium-ion batteries, Adv. Funct. Mater. 33 (2023), https://doi.org/10.1002/adfm.202210725.
[40] Y. Yang, J. Zhou, L. Wang, Z. Jiao, M. Xiao, Q.-A. Huang, M. Liu, Q. Shao, X. Sun, J. Zhang, Prussian blue and its analogues as cathode materials for Na-, K-, Mg-,

Ca-, Zn- and Al-ion batteries, Nano Energy (2022) 99, https://doi.org/10.1016/j.nanoen.2022.107424.
[41] Y. Zeng, J. Xu, Y. Wang, S. Li, D. Luan, X.W. (David) Lou, Formation of CuMn prussian blue analog double-shelled nanoboxes toward long-life Zn-ion batteries, Angew. Chem. Int. Ed. 61 (2022), https://doi.org/10.1002/anie.202212031.
[42] Y. Sun, Z. Xu, X. Xu, Y. Nie, J. Tu, A. Zhou, J. Zhang, L. Qiu, F. Chen, J. Xie, T. Zhu, X. Zhao, Low-cost and long-life Zn/Prussian blue battery using a water-in-ethanol electrolyte with a normal salt concentration, Energy Storage Mater. 48 (2022) 192–204, https://doi.org/10.1016/j.ensm.2022.03.023.
[43] M. Jiang, Z. Hou, L. Ren, Y. Zhang, J.-G. Wang, Prussian blue and its analogues for aqueous energy storage: from fundamentals to advanced devices, Energy Storage Mater. 50 (2022) 618–640, https://doi.org/10.1016/j.ensm.2022.06.006.
[44] G. Liang, J. Zhu, B. Yan, Q. Li, A. Chen, Z. Chen, X. Wang, B. Xiong, J. Fan, J. Xu, C. Zhi, Gradient fluorinated alloy to enable highly reversible Zn-metal anode chemistry, Energy Environ. Sci. 15 (2022) 1086–1096, https://doi.org/10.1039/d1ee03749h.
[45] J.-L. Yang, J. Li, J.-W. Zhao, K. Liu, P. Yang, H.J. Fan, Stable zinc anodes enabled by a zincophilic polyanionic hydrogel layer, Adv. Mater. 34 (2022), https://doi.org/10.1002/adma.202202382.
[46] P. Xue, C. Guo, L. Li, H. Li, D. Luo, L. Tan, Z. Chen, A MOF-derivative decorated hierarchical porous host enabling ultrahigh rates and superior long-term cycling of dendrite-free Zn metal anodes, Adv. Mater. 34 (2022), https://doi.org/10.1002/adma.202110047.
[47] P. Wang, S. Liang, C. Chen, X. Xie, J. Chen, Z. Liu, Y. Tang, B. Lu, J. Zhou, Spontaneous construction of nucleophilic carbonyl-containing interphase toward ultrastable zinc-metal anodes, Adv. Mater. 34 (2022), https://doi.org/10.1002/adma.202202733.
[48] Y. Zhang, Z. Cao, S. Liu, Z. Du, Y. Cui, J. Gu, Y. Shi, B. Li, S. Yang, Charge-enriched strategy based on MXene-based polypyrrole layers toward dendrite-free zinc metal anodes, Adv. Energy Mater. 12 (2022), https://doi.org/10.1002/aenm.202103979.
[49] D. Wang, Q. Li, Y. Zhao, H. Hong, H. Li, Z. Huang, G. Liang, Q. Yang, C. Zhi, Insight on organic molecules in aqueous Zn-ion batteries with an emphasis on the Zn anode regulation, Adv. Energy Mater. 12 (2022), https://doi.org/10.1002/aenm.202102707.
[50] K. Guan, L. Tao, R. Yang, H. Zhang, N. Wang, H. Wan, J. Cui, J. Zhang, H. Wang, H. Wang, Anti-corrosion for reversible zinc anode via a hydrophobic interface in aqueous zinc batteries, Adv. Energy Mater. 12 (2022), https://doi.org/10.1002/aenm.202103557.
[51] M. Liu, Q. Zhao, H. Liu, J. Yang, X. Chen, L. Yang, Y. Cui, W. Huang, W. Zhao, A. Song, Y. Wang, S. Ding, Y. Song, G. Qian, H. Chen, F. Pan, Tuning phase evolution of β-MnO_2 during microwave hydrothermal synthesis for high-performance aqueous Zn ion battery, Nano Energy 64 (2019) 103942, https://doi.org/10.1016/j.nanoen.2019.103942.
[52] W. Yuan, X. Nie, G. Ma, M. Liu, Y. Wang, S. Shen, N. Zhang, Realizing textured zinc metal anodes through regulating electrodeposition current for aqueous zinc batteries, Angew. Chem. Int. Ed. 62 (2023) e202218386, https://doi.org/10.1002/anie.202218386.
[53] F. ShakeriHosseinabad, B. Frost, S. Said, C. Xu, D. Behnoudfar, K. Amini, D. Momodu, N. Mahinpey, P. Egberts, T.S. Miller, E.P.L. Roberts, Electrode materials for enhancing the performance and cycling stability of zinc iodide flow batteries at high current densities, Acs Appl. Mater. Interfaces 15 (2023) 34711–34725, https://doi.org/10.1021/acsami.3c03785.
[54] N. Zhang, X. Chen, M. Yu, Z. Niu, F. Cheng, J. Chen, Materials chemistry for rechargeable zinc-ion batteries, Chem. Soc. Rev. 49 (2020) 4203–4219, https://doi.org/10.1039/c9cs00349e.
[55] W. Sun, F. Wang, B. Zhang, M. Zhang, V. Küpers, X. Ji, C. Theile, P. Bieker, K. Xu, C. Wang, M. Winter, A rechargeable zinc-air battery based on zinc peroxide chemistry, Science 371 (2021) 46–51, https://doi.org/10.1126/science.abb9554.
[56] G. Li, W. Chen, H. Zhang, Y. Gong, F. Shi, J. Wang, R. Zhang, G. Chen, Y. Jin, T. Wu, Z. Tang, Y. Cui, Membrane-free Zn/MnO_2 flow battery for large-scale energy storage, Adv. Energy Mater. 10 (2020) 1902085, https://doi.org/10.1002/aenm.201902085.
[57] X. Liu, H. Euchner, M. Zarrabeitia, X. Gao, G.A. Elia, A. Groß, S. Passerini, Operando pH measurements decipher H^+/Zn^{2+} intercalation chemistry in high-performance aqueous Zn/δ-V_2O_5 batteries, Acs Energy Lett 5 (2020) 2979–2986, https://doi.org/10.1021/acsenergylett.0c01767.
[58] J. Yang, R. Zhao, Y. Wang, Z. Hu, Y. Wang, A. Zhang, C. Wu, Y. Bai, Insights on artificial interphases of Zn and electrolyte: protection mechanisms, constructing techniques, applicability, and prospective, Adv. Funct. Mater. 33 (2023) 2213510, https://doi.org/10.1002/adfm.202213510.
[59] D. Chao, W. Zhou, F. Xie, C. Ye, H. Li, M. Jaroniec, S.-Z. Qiao, Roadmap for advanced aqueous batteries: from design of materials to applications, Sci. Adv. 6 (2020) eaba4098, https://doi.org/10.1126/sciadv.aba4098.
[60] Q. Cao, Y. Gao, J. Pu, A.M. Elshahawy, C. Guan, Materials and structural design for preferable Zn deposition behavior toward stable Zn anodes, Smartmat (2023) e1194, https://doi.org/10.1002/smm2.1194.
[61] Y. Gong, B. Wang, H. Ren, D. Li, D. Wang, H. Liu, S. Dou, Recent advances in structural optimization and surface modification on current collectors for high-performance zinc anode: principles, strategies, and challenges, Nano-Micro Lett 15 (2023) 208, https://doi.org/10.1007/s40820-023-01177-4.
[62] C. Zhu, P. Li, G. Xu, H. Cheng, G. Gao, Recent progress and challenges of Zn anode modification materials in aqueous Zn-ion batteries, Coord. Chem. Rev. 485 (2023) 215142, https://doi.org/10.1016/j.ccr.2023.215142.
[63] L.N. Bengoa, P. Pary, P.R. Seré, M.S. Conconi, W.A. Egli, Dendritic zinc growth in acid electrolyte: effect of the pH, J. Mater. Eng. Perform. 27 (2018) 1103–1108, https://doi.org/10.1007/s11665-018-3139-7.
[64] J. Hao, X. Li, S. Zhang, F. Yang, X. Zeng, S. Zhang, G. Bo, C. Wang, Z. Guo, Designing dendrite-free zinc anodes for advanced aqueous zinc batteries, Adv. Funct. Mater. 30 (2020), https://doi.org/10.1002/adfm.202001263.
[65] T. Wang, C. Li, X. Xie, B. Lu, Z. He, S. Liang, J. Zhou, Anode materials for aqueous zinc ion batteries: mechanisms, properties, and perspectives, ACS Nano 14 (2020) 16321–16347, https://doi.org/10.1021/acsnano.0c07041.
[66] A.R. Mainar, E. Iruin, L.C. Colmenares, A. Kvasha, I. de Meatza, M. Bengoechea, O. Leonet, I. Boyano, Z. Zhang, J.A. Blazquez, An overview of progress in electrolytes for secondary zinc-air batteries and other storage systems based on zinc, J. Energy Storage 15 (2018) 304–328, https://doi.org/10.1016/j.est.2017.12.004.
[67] B. Lee, H.R. Seo, H.R. Lee, C.S. Yoon, J.H. Kim, K.Y. Chung, B.W. Cho, S.H. Oh, Critical role of pH evolution of electrolyte in the reaction mechanism for rechargeable zinc batteries, ChemSusChem 9 (2016) 2948–2956, https://doi.org/10.1002/cssc.201600702.
[68] G. Fang, C. Zhu, M. Chen, J. Zhou, B. Tang, X. Cao, X. Zheng, A. Pan, S. Liang, Suppressing manganese dissolution in potassium manganate with rich oxygen defects engaged high-energy-density and durable aqueous zinc-ion battery, Adv. Funct. Mater. 29 (2019) 1808375, https://doi.org/10.1002/adfm.201808375.
[69] A.M. Engstrom, F.M. Doyle, Exploring the cycle behavior of electrodeposited vanadium oxide electrochemical capacitor electrodes in various aqueous environments, J. Power Sources 228 (2013) 120–131, https://doi.org/10.1016/j.jpowsour.2012.11.075.
[70] G. Li, L. Sun, S. Zhang, C. Zhang, H. Jin, K. Davey, G. Liang, S. Liu, J. Mao, Z. Guo, Developing cathode materials for aqueous zinc ion batteries: challenges and practical prospects, Adv. Funct. Mater. (2023) 2301291, https://doi.org/10.1002/adfm.202301291.
[71] X. Chen, W. Li, D. Reed, X. Li, X. Liu, On energy storage chemistry of aqueous zn-ion batteries: from cathode to anode, Electrochem. Energy Rev. 6 (2023) 33, https://doi.org/10.1007/s41918-023-00194-6.
[72] D. Wu, L.M. Housel, S.J. Kim, N. Sadique, C.D. Quilty, L. Wu, R. Tappero, S. L. Nicholas, S. Ehrlich, Y. Zhu, A.C. Marschilok, E.S. Takeuchi, D.C. Bock, K. J. Takeuchi, Quantitative temporally and spatially resolved X-ray fluorescence microprobe characterization of the manganese dissolution-deposition mechanism in aqueous Zn/α-MnO_2 batteries, Energy Environ. Sci. 13 (2020) 4322–4333, https://doi.org/10.1039/D0EE02168G.
[73] L. Cao, D. Li, E. Hu, J. Xu, T. Deng, L. Ma, Y. Wang, X.-Q. Yang, C. Wang, Solvation structure design for aqueous Zn metal batteries, J. Am. Chem. Soc. 142 (2020) 21404–21409, https://doi.org/10.1021/jacs.0c09794.
[74] C. Liu, X. Chi, Q. Han, Y. Liu, A high energy density aqueous battery achieved by dual dissolution/deposition reactions separated in acid-alkaline electrolyte, Adv. Energy Mater. 10 (2020) 1903589, https://doi.org/10.1002/aenm.201903589.
[75] M. Na, Y. Oh, H.R. Byon, Effects of Zn^{2+} and H^+ association with naphthalene diimide electrodes for aqueous Zn-ion batteries, Chem. Mater. 32 (2020) 6990–6997, https://doi.org/10.1021/acs.chemmater.0c02357.
[76] J. Yan, E.H. Ang, Y. Yang, Y. Zhang, M. Ye, W. Du, C.C. Li, High-voltage zinc-ion batteries: design strategies and challenges, Adv. Funct. Mater. 31 (2021) 2010213, https://doi.org/10.1002/adfm.202010213.
[77] C. Zhong, B. Liu, J. Ding, X. Liu, Y. Zhong, Y. Li, C. Sun, X. Han, Y. Deng, N. Zhao, W. Hu, Decoupling electrolytes towards stable and high-energy rechargeable aqueous zinc–manganese dioxide batteries, Nat. Energy 5 (2020) 440–449, https://doi.org/10.1038/s41560-020-0584-y.
[78] G.G. Yadav, M. Weiner, A. Upreti, J. Huang, T.N. Lambert, D.J. Arnot, N. B. Schorr, N.S. Bell, D. Turney, B. Hawkins, X. Wei, M. Lim, S. Banerjee, The advent of membrane-less zinc-anode aqueous batteries with lithium battery-like voltage, Mater. Horiz. 9 (2022) 2160–2171, https://doi.org/10.1039/D2MH00280A.
[79] G.G. Yadav, D. Turney, J. Huang, X. Wei, S. Banerjee, Breaking the 2V barrier in aqueous zinc chemistry: creating 2.45 and 2.8V MnO_2–Zn aqueous batteries, Acs Energy Lett 4 (2019) 2144–2146, https://doi.org/10.1021/acsenergylett.9b01643.
[80] D. Chao, C. Ye, F. Xie, W. Zhou, Q. Zhang, Q. Gu, K. Davey, L. Gu, S. Qiao, Atomic engineering catalyzed MnO_2 electrolysis kinetics for a hybrid aqueous battery with high power and energy density, Adv. Mater. 32 (2020) 2001894, https://doi.org/10.1002/adma.202001894.
[81] M. Liu, L. Yao, Y. Ji, M. Zhang, Y. Gan, Y. Cai, H. Li, W. Zhao, Y. Zhao, Z. Zou, R. Qin, Y. Wang, L. Liu, H. Liu, K. Yang, T.S. Miller, F. Pan, J. Yang, Nanoscale ultrafine zinc metal anodes for high stability aqueous zinc ion batteries, Nano Lett. 23 (2023) 541–549, https://doi.org/10.1021/acs.nanolett.2c03919.
[82] A. Naveed, H. Yang, J. Yang, Y. Nuli, J. Wang, Highly reversible and rechargeable safe Zn batteries based on a triethyl phosphate electrolyte, Angew. Chem. Int. Ed. 58 (2019) 2760–2764, https://doi.org/10.1002/anie.201813223.
[83] D. Chao, W. Zhou, C. Ye, Q. Zhang, Y. Chen, L. Gu, K. Davey, S.-Z. Qiao, An electrolytic Zn-MnO_2 battery for high-voltage and scalable energy storage, Angew. Chem. Int. Ed. 58 (2019) 7823–7828, https://doi.org/10.1002/anie.201904174.
[84] W. Zhang, Y. Dai, R. Chen, Z. Xu, J. Li, W. Zong, H. Li, Z. Li, Z. Zhang, J. Zhu, F. Guo, X. Gao, Z. Du, J. Chen, T. Wang, G. He, I.P. Parkin, Highly reversible zinc metal anode in a dilute aqueous electrolyte enabled by a pH buffer additive, Angew. Chem. Int. Ed. 62 (2023) e202212695, https://doi.org/10.1002/anie.202212695.
[85] R. Chen, W. Zhang, Q. Huang, C. Guan, W. Zong, Y. Dai, Z. Du, Z. Zhang, J. Li, F. Guo, X. Gao, H. Dong, J. Zhu, X. Wang, G. He, Trace amounts of triple-

functional additives enable reversible aqueous zinc-ion batteries from a comprehensive perspective, Nano-Micro Lett 15 (2023) 81, https://doi.org/10.1007/s40820-023-01050-4.
[86] L. Yao, C. Hou, M. Liu, H. Chen, Q. Zhao, Y. Zhao, Y. Wang, L. Liu, Z. Yin, J. Qiu, S. Li, R. Qin, F. Pan, Ultra-stable Zn anode enabled by fiber-directed ion migration using mass-producible separator, Adv. Funct. Mater. 33 (2023) 2209301, https://doi.org/10.1002/adfm.202209301.
[87] D. Yang, X. Wu, L. He, Z. Sun, H. Zhao, M. Wang, Y. Wang, Y. Wei, Physicochemical synergistic separator coating induces uniform and rapid deposition of Li and Zn ions, Nano Lett. 23 (2023) 336–343, https://doi.org/10.1021/acs.nanolett.2c04613.
[88] Q. Xu, Q.-X. Xie, T. Xue, G. Cheng, J.-D. Wu, L. Ning, X.-H. Yan, Y.-J. Lu, Z.-L. Zou, B.-P. Wang, F.-L. Han, Salt Bridge-intermediated three phase decoupling electrolytes for high voltage electrolytic aqueous Zinc-Manganese dioxides battery, Chem. Eng. j. 451 (2023) 138775, https://doi.org/10.1016/j.cej.2022.138775.
[89] Z. Li, L. Ye, G. Zhou, W. Xu, K. Zhao, X. Zhang, S. Hong, T. Ma, M.-C. Li, C. Liu, C. Mei, A water-gating and zinc-sieving lignocellulose nanofiber separator for dendrite-free rechargeable aqueous zinc ion battery, Chem. Eng. j. 457 (2023) 141160, https://doi.org/10.1016/j.cej.2022.141160.
[90] D. Han, Z. Wang, H. Lu, H. Li, C. Cui, Z. Zhang, R. Sun, C. Geng, Q. Liang, X. Guo, Y. Mo, X. Zhi, F. Kang, Z. Weng, Q.-H. Yang, A self-regulated interface toward highly reversible aqueous zinc batteries, Adv. Energy Mater. 12 (2022) 2102982, https://doi.org/10.1002/aenm.202102982.
[91] C. Lin, X. Yang, P. Xiong, H. Lin, L. He, Q. Yao, M. Wei, Q. Qian, Q. Chen, L. Zeng, High-rate, large capacity, and long life dendrite-free zn metal anode enabled by trifunctional electrolyte additive with a wide temperature range, Adv. Sci. 9 (2022), https://doi.org/10.1002/advs.202201433.
[92] X. Zhao, X. Zhang, N. Dong, M. Yan, F. Zhang, K. Mochizuki, H. Pan, Advanced buffering acidic aqueous electrolytes for ultra-long life aqueous zinc-ion batteries, Small 18 (2022) 2200742, https://doi.org/10.1002/smll.202200742.
[93] M. Zhang, H. Hua, P. Dai, Z. He, L. Han, P. Tang, J. Yang, P. Lin, Y. Zhang, D. Zhan, J. Chen, Y. Qiao, C.C. Li, J. Zhao, Y. Yang, Dynamically interfacial pH-buffering effect enabled by *N* -methylimidazole molecules as spontaneous proton pumps toward highly reversible zinc-metal anodes, Adv. Mater. (2023) 2208630, https://doi.org/10.1002/adma.202208630.
[94] Y. Song, P. Ruan, C. Mao, Y. Chang, L. Wang, L. Dai, P. Zhou, B. Lu, J. Zhou, Z. He, Metal–organic frameworks functionalized separators for robust aqueous zinc-ion batteries, Nano-Micro Lett 14 (2022) 218, https://doi.org/10.1007/s40820-022-00960-z.
[95] Y. Dai, J. Li, L. Chen, K. Le, Z. Cai, Q. An, L. Zhang, L. Mai, Generating H^+ in catholyte and OH^- in anolyte: an approach to improve the stability of aqueous zinc-ion batteries, Acs Energy Lett 6 (2021) 684–686, https://doi.org/10.1021/acsenergylett.0c02683.
[96] X. Yang, W. Wu, Y. Liu, Z. Lin, X. Sun, Chitosan modified filter paper separators with specific ion adsorption to inhibit side reactions and induce uniform Zn deposition for aqueous Zn batteries, Chem. Eng. J. 450 (2022) 137902, https://doi.org/10.1016/j.cej.2022.137902.
[97] G. Guo, X. Tan, K. Wang, L. Zheng, H. Zhang, Regulating zinc deposition behaviors by functional cotton textiles as separators for aqueous zinc-metal batteries, J. Power Sources 553 (2023) 232321, https://doi.org/10.1016/j.jpowsour.2022.232321.
[98] J. Fu, H. Wang, P. Xiao, C. Zeng, Q. Sun, H. Li, A high strength, anti-corrosion and sustainable separator for aqueous zinc-based battery by natural bamboo cellulose, Energy Storage Mater. 48 (2022), https://doi.org/10.1016/j.ensm.2022.02.052, 191-191.f6.
[99] W. Zhou, M. Chen, Q. Tian, J. Chen, X. Xu, C.-P. Wong, Cotton-derived cellulose film as a dendrite-inhibiting separator to stabilize the zinc metal anode of aqueous zinc ion batteries, Energy Storage Mater. 44 (2022) 57–65, https://doi.org/10.1016/j.ensm.2021.10.002.
[100] S. Huang, L. Hou, T. Li, Y. Jiao, P. Wu, Antifreezing hydrogel electrolyte with ternary hydrogen bonding for high-performance zinc-ion batteries, Adv. Mater. 34 (2022), https://doi.org/10.1002/adma.202110140.
[101] S. Liu, H. Zhu, B. Zhang, G. Li, H. Zhu, Y. Ren, H. Geng, Y. Yang, Q. Liu, C.C. Li, Tuning the kinetics of zinc-ion insertion/extraction in V_2O_5 by in situ polyaniline intercalation enables improved aqueous zinc-ion storage performance, Adv. Mater. 32 (2020), https://doi.org/10.1002/adma.202001113.
[102] W. Li, C. Han, Q. Gu, S.-L. Chou, J.-Z. Wang, H.-K. Liu, S.-X. Dou, Electron delocalization and dissolution-restraint in vanadium oxide superlattices to boost electrochemical performance of aqueous zinc-ion batteries, Adv. Energy Mater. 10 (2020), https://doi.org/10.1002/aenm.202001852.
[103] X. Zhao, L. Mao, Q. Cheng, F. Liao, G. Yang, X. Lu, L. Chen, Interlayer engineering of preintercalated layered oxides as cathode for emerging multivalent metal-ion batteries: zinc and beyond, Energy Storage Mater. 38 (2021) 397–437, https://doi.org/10.1016/j.ensm.2021.03.005.
[104] R. Li, F. Xing, T. Li, H. Zhang, J. Yan, Q. Zheng, X. Li, Intercalated polyaniline in V_2O_5 as a unique vanadium oxide bronze cathode for highly stable aqueous zinc ion battery, Energy Storage Mater. 38 (2021) 590–598, https://doi.org/10.1016/j.ensm.2021.04.004.
[105] C. Kim, B.Y. Ahn, T.-S. Wei, Y. Jo, S. Jeong, Y. Choi, I.-D. Kim, J.A. Lewis, High-power aqueous zinc-ion batteries for customized electronic devices, ACS Nano 12 (2018) 11838–11846, https://doi.org/10.1021/acsnano.8b02744.
[106] H.-Y. Shi, Y.-J. Ye, K. Liu, Y. Song, X. Sun, A long-cycle-life self-doped polyaniline cathode for rechargeable aqueous zinc batteries, Angew. Chem. Int. Ed. 57 (2018) 16359–16363, https://doi.org/10.1002/anie.201808886.
[107] Y. Liu, Z. Dai, W. Zhang, Y. Jiang, J. Peng, D. Wu, B. Chen, W. Wei, X. Chen, Z. Liu, Z. Wang, F. Han, D. Ding, L. Wang, L. Li, Y. Yang, Y. Huang, Sulfonic-group-grafted Ti_3C_2Tx MXene: a silver bullet to settle the instability of polyaniline toward high-performance Zn-ion batteries, ACS Nano 15 (2021) 9065–9075, https://doi.org/10.1021/acsnano.1c02215.
[108] N. Zhao, Y. Zhang, Z. Zhang, C. Han, Y. Liang, J. Li, X. Wang, L. Dai, L. Wang, Z. He, Polyaniline functionalized separator as synergistic medium for aqueous zinc-ion batteries, J. Colloid Interface Sci. 642 (2023) 421–429, https://doi.org/10.1016/j.jcis.2023.03.184.
[109] B. Li, S. Liu, Y. Geng, C. Mao, L. Dai, L. Wang, S.C. Jun, B. Lu, Z. He, J. Zhou, Achieving stable zinc metal anode via polyaniline interface regulation of Zn ion flux and desolvation, Adv. Funct. Mater. (2023) 2214033, https://doi.org/10.1002/adfm.202214033.
[110] T. Wang, P. Wang, L. Pan, Z. He, L. Dai, L. Wang, S. Liu, S.C. Jun, B. Lu, S. Liang, J. Zhou, Stabling zinc metal anode with polydopamine regulation through dual effects of fast desolvation and ion confinement, Adv. Energy Mater. 13 (2023) 2203523, https://doi.org/10.1002/aenm.202203523.
[111] F. Li, D. Ma, K. Ouyang, M. Yang, J. Qiu, J. Feng, Y. Wang, H. Mi, S. Sun, L. Sun, C. He, P. Zhang, A theory-driven complementary interface effect for fast-kinetics and ultrastable Zn metal anodes in aqueous/solid electrolytes, Adv. Energy Mater. 13 (2023), https://doi.org/10.1002/aenm.202204365.
[112] L. Yang, Q. Ma, Y. Yin, D. Luo, Y. Shen, H. Dou, N. Zhu, R. Feng, Y. Kong, A. Yu, B. Cheng, X. Wang, Z. Chen, Construction of desolvated ionic COF artificial SEI layer stabilized Zn metal anode by in-situ electrophoretic deposition, Nano Energy 117 (2023), https://doi.org/10.1016/j.nanoen.2023.108799.
[113] F. Ling, L. Wang, F. Liu, M. Ma, S. Zhang, X. Rui, Y. Shao, Y. Yang, S. He, H. Pan, X. Wu, Y. Yao, Y. Yu, Multi-scale structure engineering of $ZnSnO_3$ for ultra-long-life aqueous zinc-metal batte, Adv. Mater. 35 (2023) 2208764, https://doi.org/10.1002/adma.202208764.
[114] M. Liu, L. Yang, H. Liu, A. Amine, Q. Zhao, Y. Song, J. Yang, K. Wang, F. Pan, Artificial solid-electrolyte interface facilitating dendrite-free zinc metal anodes via nanowetting effect, Acs Appl. Mater. Interfaces 11 (2019) 32046–32051, https://doi.org/10.1021/acsami.9b11243.
[115] D. Li, Y. Ouyang, H. Lu, Y. Xie, S. Guo, Q. Zeng, Y. Xiao, Q. Zhang, S. Huang, Manipulating Lewis acid–base interactions in metal-organic frameworks for optimizing zinc-ion diffusion, deposition, and reaction behaviors, Mater. Today Chem. 32 (2023) 101629, https://doi.org/10.1016/j.mtchem.2023.101629.
[116] K. Qi, W. Zhu, X. Zhang, M. Liu, H. Ao, X. Wu, Y. Zhu, Enamel-like layer of nanohydroxyapatite stabilizes Zn metal anodes by ion exchange adsorption and electrolyte pH regulation, ACS Nano 16 (2022) 9461–9471, https://doi.org/10.1021/acsnano.2c02448.
[117] J. Ke, Z. Wen, Y. Yang, R. Tang, Y. Tang, M. Ye, X. Liu, Y. Zhang, C.C. Li, Tailoring anion association strength through polycation-anion coordination mechanism in imidazole polymeric ionic liquid-based artificial interphase toward durable Zn metal anodes, Adv. Funct. Mater. 33 (2023) 2301129, https://doi.org/10.1002/adfm.202301129.
[118] X. Zeng, K. Xie, S. Liu, S. Zhang, J. Hao, J. Liu, W.K. Pang, J. Liu, P. Rao, Q. Wang, J. Mao, Z. Guo, Bio-inspired design of an in situ multifunctional polymeric solid-electrolyte interphase for Zn metal anode cycling at 30mA cm^{-2} and 30mA h cm^{-2}, Energy Environ. Sci. 14 (2021) 5947–5957, https://doi.org/10.1039/d1ee01851e.
[119] X. Zeng, J. Mao, J. Hao, J. Liu, S. Liu, Z. Wang, Y. Wang, S. Zhang, T. Zheng, J. Liu, P. Rao, Z. Guo, Electrolyte design for in situ construction of highly Zn^{2+}-conductive solid electrolyte interphase to enable high-performance aqueous Zn-ion batteries under practical conditions, Adv. Mater. 33 (2021).
[120] L. Ma, Q. Li, Y. Ying, F. Ma, S. Chen, Y. Li, H. Huang, C. Zhi, Toward practical high-areal-capacity aqueous zinc-metal batteries: quantifying hydrogen evolution and a solid-ion conductor for stable zinc anodes, Adv. Mater. 33 (2021), https://doi.org/10.1002/adma.202007406.
[121] J. Hao, B. Li, X. Li, X. Zeng, S. Zhang, F. Yang, S. Liu, D. Li, C. Wu, Z. Guo, An in-depth study of Zn metal surface chemistry for advanced aqueous Zn-ion batteries, Adv. Mater. 32 (2020), https://doi.org/10.1002/adma.202003021.
[122] Y. Chu, S. Zhang, S. Wu, Z. Hu, G. Cui, J. Luo, In situ built interphase with high interface energy and fast kinetics for high performance Zn metal anodes, Energy Environ. Sci. 14 (2021) 3609–3620, https://doi.org/10.1039/d1ee00308a.
[123] X. Guo, Z. Zhang, J. Li, N. Luo, G.-L. Chai, T.S. Miller, F. Lai, P. Shearing, D.J. L. Brett, D. Han, Z. Weng, G. He, I.P. Parkin, Alleviation of dendrite formation on zinc anodes via electrolyte additives, Acs Energy Lett. 6 (2021) 395–403, https://doi.org/10.1021/acsenergylett.0c02371.
[124] Z. Zhang, S. Said, K. Smith, Y.S. Zhang, G. He, R. Jervis, P.R. Shearing, T.S. Miller, D.J. Brett, Dendrite suppression by anode polishing in zinc-ion batteries, J. Mater. Chem. A 9 (2021) 15355–15362.
[125] X. Yang, C. Li, Z. Sun, S. Yang, Z. Shi, R. Huang, B. Liu, S. Li, Y. Wu, M. Wang, Y. Su, S. Dou, J. Sun, Interfacial manipulation via in situ grown ZnSe cultivator toward highly reversible Zn metal anodes, Adv. Mater. 33 (2021), https://doi.org/10.1002/adma.202105951.